Journal of Hydrology 649 (2025) 132411

Contents lists available at ScienceDirect

Journal of Hydrology

journal homepage: www.elsevier.com/locate/jhydrol

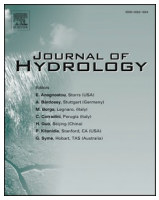

Research papers

# Energy balance modelling of snow and ice melt for the Naltar catchment (Karakoram, Pakistan) in future climate

Muhammad Usman Liaqat [a,b,*], Ana Casanueva [c,d], Rubina Ansari [a], Giovanna Grossi [a], Roberto Ranzi [a]

[a] Department of Civil, Environmental, Architectural Engineering and Mathematics, Università degli Studi di Brescia, Via Branze, 43, 25123 Brescia BS, Italy
[b] Research Institute for Geo-Hydrological Protection, National Research Council of Italy, Via Madonna Alta, 126, 06128 Perugia Italy
[c] Dept. Matemática Aplicada y Ciencias de la Computación (MACC), Universidad de Cantabria, Santander Spain
[d] Grupo de Ciencia de Datos para el Clima (CD-Clim), Unidad Asociada al CSIC, Santander, Spain

ARTICLE INFO

*Keywords:*
Climate Change
Hydrological Modelling
Upper Indus Basin
CORDEX South Asia
Regional Climate Models
Karakoram anomaly

ABSTRACT

High Mountain Asia (HMA), including the Hindu Kush-Karakoram Himalayas (HKH) is one of the world's key "water towers", with the resources supporting hundreds of millions of people. Currently, this region is experiencing significant demographic and socio-economic growth. Reliable hydrological projections of the future supply of water resources are essential, given the likelihood that water resources demand will continue to increase. In this study, CORDEX South Asia (CORDEX-WAS44) regional climate models (RCMs) and the Physically Based Distributed Snow Land and Ice Model, that was calibrated with hourly meteorological data and daily runoff over eight years of monitoring period, are employed in the Naltar catchment located in the Hunza river basin, Upper Indus Basin, Pakistan to project glacio-hydrological regimes in the future climate. For each of the CORDEX-WAS44 simulations, climate change signals for near future (2040–2059) and far future (2080–2099) under three Representative Concentration Pathways (RCPs) namely RCP2.6, RCP4.5, and RCP8.5 are presented with respect to the corresponding present climate (1991–2010). Results show overall significant increases in mean temperature between (+0.9 to + 6.0 °C, depending upon the scenario) and total precipitation (+6 to + 29 %) from April to September by the end of the century for RCP2.6, RCP4.5, and RCP8.5. The projected simulations of energy and mass balance indicate that snow and ice melt rate will increase consistently in both future periods with an earlier timing of the snowmelt as it appears in June in the near future (2040–2059) and in May in the far future (2080–2099) under the high emission scenario (RCP8.5). The increase in temperature, precipitation and winter snowpack changes are also expected to have a substantial impact on the hydrological regime in the Naltar catchment, with a peak flow occurring one to two months earlier and a total by 2090 and a decrease of total runoff in the monsoon season by –3 to –24 % in the near and far future, respectively, under RCP 8.5 scenario and more neutral changes (–2 to + 3 %) according to RCP 4.5. Based on these results and the discussion above, water availability in the Naltar catchment will be uncertain by the end of the century.

## 1. Introduction

Snow and glaciers are the primary source of freshwater resources in Hindu Kush Himalaya and Karakoram (HKH) especially in Pakistan, where they release a substantial amount of water supply during the whole year. Early nineteenth-century explorations suggested that the Karakoram glaciers behaved in a peculiar manner with climate change (Godwin-Austen, 1864; Hayden, 1907). Hewitt (2005) coined the term 'Karakoram Anomaly', the stability or abnormal growth of glaciers in the central Karakoram, as opposed to glaciers retreating in nearby mountain ranges such as the Himalayan range (Xiang et al., 2024) or in other mountain ranges around the world such as the Alps (Paul et al., 2014; Carturan et al., 2016), and the Canadian Rockies (Fang and Pomeroy, 2023). Comparing the evolution of Karakoram's glaciers to those of other regions on the Earth, modern observations are more conclusive (Minora et al., 2013; Bishop et al., 2014; Minora et al., 2016; Berthier and Brun, 2019). However, in light of current global warming, it appears unlikely that the Karakoram Anomaly will persist in the long

* Corresponding author.
*E-mail address:* usmanliaqat0321@gmail.com (M.U. Liaqat).

https://doi.org/10.1016/j.jhydrol.2024.132411
Received 18 August 2023; Received in revised form 15 October 2024; Accepted 9 November 2024
Available online 25 November 2024

term (Farinotti et al. 2020), resulting in a substantial glaciers' retreat in Karakoram as in the rest of the world. Thus, it is imperative to examine this phenomenon especially at sub-regional scale where glacier surging occurred two years ago (Dawn, 2021).

The hydrological setup of Pakistan is marked as a climate change "hotspot". In the last two–three decades, Pakistan has also become one of the most vulnerable regions coping with severe floods, droughts, and storm events (Hussain and Mumtaz, 2014; Nanditha et al., 2023; Chen et al., 2024; Ansari et al., 2024). The temperature rise due to global warming further enhances elevation-dependent warming and increases early snow melt rate during pre-monsoon which leads to significant impacts on the magnitude, and timing of generated flows (Hasson and Böhner, 2019; Ansari et al., 2022). It is found that precipitation and streamflow also exhibit significant positive observed trends especially during winter and pre-monsoon, while slightly decreasing in the summer season (Liaqat et al., 2022). It is estimated that a combined hydropower capacity of 51.2 MW will be operational by 2030 on the Naltar river, which not only helps to control water from glacier melt but also meets energy demands in Gilgit-Baltistan. Hence, it is crucial to understand how glaciers are responding to climate change and its effect on the region's snow cover dynamics and hydrological systems' response.

Global climate models (GCMs) are the primary source of knowledge about future climate changes. These models offer a simplified form of the physical processes that connect the atmosphere, ocean, sea ice, land surface, and biogeochemical system. GCMs have a typical horizontal resolution of approximately 100x100km resolution. Numerous studies have made use of hydrological models in combination with GCMs to assess future changes in the hydrological cycle in mountain basins worldwide (see e.g., Fang and Pomeroy, 2023) and specifically in the HKH. Tahir et al. (2011) used the snowmelt runoff model (SRM) integrated with MODIS snow cover product to simulate daily runoff under climate change conditions in the glacierized Hunza basin, in the Upper Indus Basin (UIB). They found that a) an increase of 1 °C in air temperature with no change in precipitation and snow cover is expected to induce a rise in summer runoff up to 33 % and b) under far future period the +2 °C to +4 °C rise in mean temperature with 20 % increase in snow cover area is expected to increase future streamflow by 100 %. Laghari et al. (2012) examined current and future water availability in the Indus basin. They concluded that water availability will increase in the near future, while it will decrease in the long term.

Lutz et al. (2016) found a significant increase in winter precipitation in the Karakoram, but the rapid increase in temperature, especially at high altitude zones, leads to more precipitation falling as rain instead of snow. Thus, reduced snow precipitation during the accumulation period and rapid melting of snowpack from subsurface layers also result in early exposure of glacier surfaces, which enhances the melting of glaciers in the basin. Hasson et al. (2019) projected water availability in three important Himalayan watersheds (Kabul, Indus and Jhelum). They found that if glaciers remain in current conditions, future water availability would increase by 34 % and 43 % on average under global warming levels of +1.5 °C and +2.0 °C, respectively. However, if the glacierized area in the Himalayan watersheds retreats by 100 %, water availability will decline up to –25 % under both warming levels. Similarly, some other studies also used different hydrological models to assess the possible impacts of climate change on the hydrological regime of the UIB (Fowler et al., 2003; Bocchiola et al., 2011; Lutz et al., 2016; Soncini et al., 2016; Atif et al., 2019; Ismail et al., 2020; Kiani et al., 2021). Despite the large availability of GCMs, their coarse resolution poses limitations for simulating physical surface processes especially in HKH, where complex topography introduces further uncertainties in climate change projections and subsequently in future water availability assessments (Hasson and Böhner, 2019).

Previous studies mainly focused on climate change impact assessments and hydro-glaciological projections at transboundary or large drainage basins (Lutz et al., 2014; Lutz et al., 2016; Kraaijenbrink et al., 2017; Bokhari et al., 2018; Zheng et al., 2018; Kiani et al., 2021; Kraaijenbrink et al., 2021; Rounce et al., 2020; Shah et al., 2020). However, water resources management decisions, especially in complex topography, take place at smaller catchments and sub-basins level (Shakoor and Ejaz, 2019). Recently, Aftab et al. (2022) also examined hydro-climatic regimes using ERA5-Land (temperature and precipitation) and newly released Coupled Model Intercomparison Project Phase 6 (CMIP6) climate projections in the Hunza basin. Even though CMIP6 provides a new generation of GCMs with higher resolution than its predecessor (CMIP5) and a new set of emissions and land use scenarios, the Physically based Distributed Snow Land and Ice Model (PDSLIM) adopted in this work is potentially able to account for more complex physical processes since also relative humidity, solar radiation, wind speed and surface pressure and a detailed modelling of topography, including shadowing, terrain and sky view factors, are involved. Further, the Naltar catchment is quite small compared to the whole Hunza basin, so it would be very difficult to capture change signals from coarse resolution GCMs.

As an alternative Regional Climate Models (RCMs), with finer spatial resolution and better parameterized small-scale atmospheric processes, are considered more reliable to simulate the regional climate (Choudhary and Dimri, 2018; Sebok et al., 2022). RCMs are commonly developed on a 50x50km or 25x25km grid on continental scales and use boundary conditions of GCMs. Processes occurring at smaller scales than the grid spacing are introduced by means of physical parameterizations. The World Climate Research Programme (WCRP) started the Coordinated Regional Downscaling Experiment (CORDEX) that developed an ensemble of regional climate change projections for 14 continental domains, including South Asia (CORDEX-WAS44), developed on a 0.44°x0.44° grid (approximately 50x50km) (Gutowski Jr et al., 2016). In the past years, different studies employed CORDEX-WAS44 simulations with integration of hydro-glaciological models to compute possible climate change and hydrological effects in HKH (Ahmad and Rasul, 2018; Azmat et al., 2020; Fatima et al., (2020); Ismail et al., 2020; Khan et al., 2020). Each study developed specific criteria for model selection before their application in future projections and impact assessments. For instance, Fatima et al. (2020) selected four CORDEX-WAS44 RCMs based on the availability of all emission scenarios (RCPs, Representative Concentration Pathways) for consistency purposes. Azmat et al. (2020) employed four CORDEX-WAS44 RCMs based on the temporal consistency of the historical simulations with observed data. Analyzing climate model performance before its application in impact assessments can also be one way to reduce the overall uncertainties, but it is still questionable if a model exhibiting good agreement with the reference data in the historical period will provide a more realistic climate projection (Knutti et al., 2010).

Bearing all these issues in mind, this study examines the performance and future evolution of glaciers in the Naltar catchment by making use of the largest possible ensemble of fine resolution RCMs combined with projected glacier extent using the PDSLIM model (Ranzi and Rosso, 1991; Ranzi et al., 2010; Grossi et al., 2013). To the authors knowledge it is the first time that different sources of future uncertainties (i.e. different RCMs, driven by different GCMs and following different emission scenarios) are used for these purposes in the Hunza river basin. As no climate model is superior to others, the use of multi-model ensembles is essential for the quantification of all aspects of model uncertainty and it has been demonstrated that combining models generally increases the skill and reliability (Tebaldi and Knutti, 2007 and references therein). Unlike previous works, we estimated climate projections at high temporal resolution, since simulated climate change signals are transferred to hourly observed meteorological variables. The PDSLIM coupled with the conceptual hydrological routing model LRM was already calibrated and validated successfully using observed hydrometric and satellite data in the Naltar catchment (Liaqat and Ranzi, 2024). The present study explores (i) the evolution of snow, ice melt and glaciers' extension using PDSLIM, (ii) future flow regimes generated by snow-glacier melt and rainfall by near future (2040–2059) and far future

(2080–2099) under a wide ensemble of RCP 2.6, RCP 4.5 and RCP 8.5 scenarios, (iii) how future changes in mass balance and extension of glaciers reveal the Karakoram anomaly and if this anomaly will continue for the Naltar basin in the future. This study aims to provide substantial understanding about future snow and ice cover dynamics and water availability for efficient water resources management and for future power generation projects in the Naltar catchment. The findings are meant to set the basis for appropriate decision making and long-term plans, as well as adaptation strategies in water resources management to deal with future changes.

## 2. Material and methods

### 2.1. Study area

Covering an area of 242.69 km$^2$, estimated by the ASTER Global Digital Elevation Model (ASTER GDEM) available at 90-m resolution, the Naltar catchment lies within high mountain ranges of Western Karakoram between 36.05° and 36.27° N and 74.08° and 74.28° E as shown in Fig.1. It is located in the Hunza basin about 42 km away from Gilgit city and 208 km from K2 (the second highest mountain in the world) in the Gilgit-Baltistan region of Pakistan (Gardezi et al., 2022). The largest part of the Naltar catchment is filled with snow-glacier cover due to the westerlies. According to the Randolph Glacier Inventory (RGI 6.0), the glacier coverage of the Naltar catchment is 42 km$^2$, with the area of the largest glacier being 19 km$^2$. The proportion of debris-covered glaciers is 9.13 %. Debris cover was detected from satellite images and incorporated in the energy balance model that considers the effect of debris cover as well. The detailed description of modelling debris cover glaciers in PDSLIM can be found in (Ranzi et al., 2004; Ranzi et al., 2010). The mean annual (2006–2016) snow coverage ranges between 93.5 % of the basin area in March and 18.31 % in September (Muhammad and Thapa, 2021). The elevation of the Naltar catchment,characterized by complex topography and deep valleys, ranges from 2270 m to 5869 m a.s.l. with a mean elevation of 4064 m a.s.l. The mean annual accumulated precipitation and temperature recorded at the Naltar station (triangle in Fig.1) are 685 mm and 6.5 °C, respectively (Liaqat et al., 2022). There are three small operational hydropower plants in the Naltar river (Naltar-II, Naltar-IV, Naltar-V) with average capacity of 2.8 MW, 18 MW, 14.4 MW, respectively. Recently, the Government of Pakistan also approved the construction of the Naltar hydropower project (Phase-III). Hence, it would be imperative to examine the evolution of future water availability in the Naltar catchment which is not only important to compute water demand for people living in downstream areas, but it is also helpful to fulfill energy demand for Naltar and surrounding areas.

### 2.2. Hydro-meteorological, satellite and snow cover measurements for the Naltar catchment

PDSLIM requires hourly meteorological data and satellite data (leaf area index (LAI) and albedo from MODIS, snow water equivalent (SWE) through Bair et al. (2020) and Global Land Cover Map by the European Space Agency (ESA) to simulate snow and ice melt and runoff production in the melting season (April-September). It is also important to mention that we used all satellite data as an initial condition in the

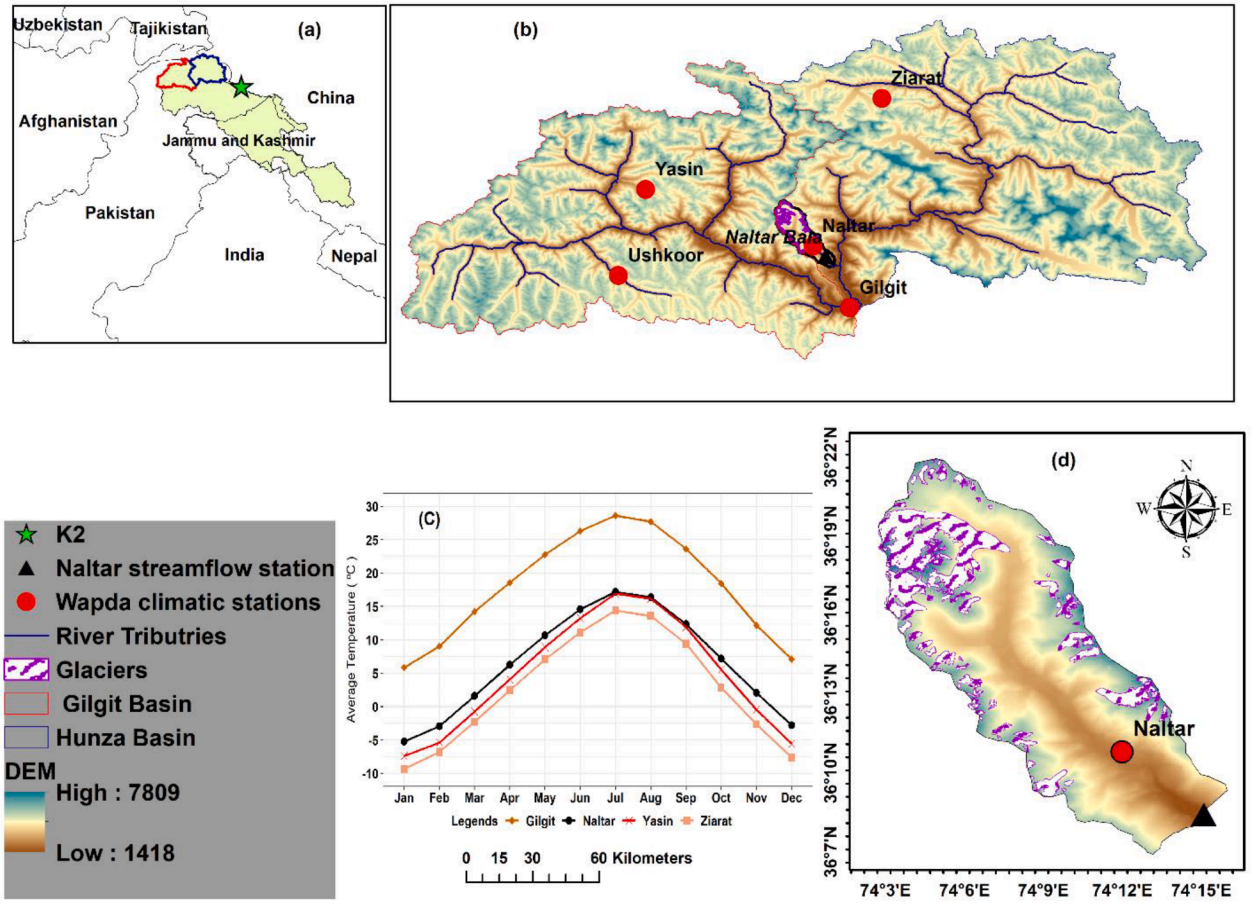


**Fig. 1.** (a) The boundary of the Upper Indus Basin (green shading) with blue and red line for Gilgit and Hunza sub-basins; (b) location of the Naltar catchment within the Hunza Basin (blue border), Gilgit Basin (red border) and hydro-meteorological stations (red circles); (c) annual cycle of mean monthly temperature from several meteorological stations and (d) a clear representation of Naltar catchment with glacier coverage.

model. The model automatically simulates for the rest of the period in each simulated year. The detailed description of using meteorological and satellite data can be found in Liaqat and Ranzi (2024). In this study, hourly meteorological data for 2006–2016 were acquired from the Water and Power development Authority (WAPDA), Pakistan for the model calibration and verification. A consistency check revealed that this dataset had some missing values for some variables at different dates and times. We selected eight (2006, 2008, 2009, 2010, 2011, 2012, 2014 and 2016) out of eleven years for which missing values amounted to less than 20 %. The remaining missing values in the selected years were estimated through multiple linear regression as used by Prabnakorn et al. (2019). The method involves developing a relationship between different sets of neighboring stations of Naltar station (see red dot in Fig.1d) and choosing one with the best coefficient of determination ($R^2$), but not less than 0.6 for precipitation, relative humidity, wind speed and solar radiation and 0.75 for temperature.

The model simulates for each grid cell the radiative, turbulent, conductive fluxes and computes heat exchange and melt. Then the observed precipitation and computed snow- and ice-melt is routed through a conceptual linear reservoirs model named LRM with lumped parameters as it can be seen in Liaqat and Ranzi (2024) to estimate daily runoff at the basin outlet hydrometric observation station of Naltar with a catchment area of 242.69 km2. Simulated runoff is separated into its surface and subsurface components.

The meteorological information required to run the fully distributed PDSLIM model consists of precipitation, air temperature, relative humidity, wind speed, solar radiation and air pressure. Air pressure values are not measured by WAPDA stations, thus these values were taken from Bair et al. (2020). Similarly, streamflow data for Naltar river were collected from WAPDA for the same time period as the meteorological observations. A detailed description of the hydro-meteorological stations considered in this study is given in Table S3, Table S4 and Fig. 1.

Details of the satellite-derived Digital Elevation Model, land use, vegetation, ice thickness and snow cover data used for the model's setup and verification are described in Liaqat and Ranzi (2024).

### 2.3. Climate model projections

Climate projections given by regional climate models (RCMs) serve as an essential input for climate change studies and impact assessments (Giorgi et al., 2009). In this study, 37 CORDEX-WAS44 RCM simulations (3 RCMs unevenly driven by 10 CMIP5 GCMs) at 0.44° (~50 km) spatial resolution were employed for the period 1991–2099 (Table 1). For each simulation, data from the gridbox over the Naltar catchment was considered.

In particular, mean daily data from six meteorological variables

**Table 1**
List of CORDEX South Asia (WAS-44) Regional Climate Model simulations, driving GCMs and available RCPs.

| RCM | RCM description | Contributing CORDEX modelling center | ID | Driving CMIP5 GCM | Contributing CMIP5 modeling center | RCP26 | RCP45 | RCP85 |
|---|---|---|---|---|---|---|---|---|
| RegCM4 | The Abdus Salam International Centre for Theoretical Physics (ICTP) Regional Climate Model version 4 (RegCM4; (Giorgi et al. 2012)) | Centre for Climate Change Research (CCCR), Indian Institute of Tropical Meteorology (IITM), India | RCM1 | CCCma-CanESM2 | Canadian Center for Climate Modelling and Analysis (CCCma), Canada | × | ✔ | ✔ |
| | | | RCM2 | CSIRO-QCCCE-CSIRO | Commonwealth Scientific and Industrial Research, Australia | × | ✔ | ✔ |
| | | | RCM3 | IPSL-IPSL-CM5A-LR | Institut Pierre Simon Laplace, France | × | ✔ | ✔ |
| | | | RCM4 | MPI-M−MPI−ESM | Max Plank Institute for Meteorology, Germany (MPI-M) | × | ✔ | ✔ |
| | | | RCM5 | NOAA-GFDL-GFDL-ESM2M | National Oceanic and Atmospheric Administration, Geophysical Fluid Dynamics Laboratory (GFDL) | × | ✔ | ✔ |
| RCA4 | Rossby Centre Regional Atmospheric Model version 4 (RCA4; (Samuelsson et al. 2011)) | Rossby Centre, Swedish Meteorological and Hydrological Institute (SMHI), Sweden | RCM6 | CCCma-CanESM2 | Canadian Center for Climate Modelling and Analysis (CCCma), Canada | × | ✔ | ✔ |
| | | | RCM7 | CNRM-CERFACS | National Centre for Meteorological Research, France | × | ✔ | ✔ |
| | | | RCM8 | CSIRO-QCCCE-CSIRO | Commonwealth Scientific and Industrial Research, Australia | × | ✔ | ✔ |
| | | | RCM9 | ICHEC-EC-EARTH | Irish Center for High-End Computing, European Consortium | ✔ | ✔ | ✔ |
| | | | RCM10 | IPSL-IPSL-CM5A-MR | Institut Pierre Simon Laplace, France | × | ✔ | ✔ |
| | | | RCM11 | MIROC-MIROC5 | Model for Interdisciplinary Research on Climate (MIROC), Japan, Agency for Marine-Earth Science and Tech | ✔ | ✔ | ✔ |
| | | | RCM12 | MOHC-HadGEM2-ES | Met Office Hadley Centre for Climate Science | ✔ | ✔ | ✔ |
| | | | RCM13 | MPI-M−MPI−ESM | Max Plank Institute for Meteorology,Germany (MPI-M) | ✔ | ✔ | ✔ |
| | | | RCM14 | NCC-NorESM1-M | Norwegian Climate Center (NCC), Norway | ✔ | ✔ | ✔ |
| | | | RCM15 | NOAA-GFDL-GFDL-ESM2M | National Oceanic and Atmospheric Administration, Geophysical Fluid Dynamics Laboratory (GFDL) | × | ✔ | ✔ |
| REMO2009 | MPI Regional model 2009 (REMO2009; (Teichmann et al. 2013) | Climate Service Center (CSC), Germany | RCM16 | MPI-M−MPI−ESM | Max Plank Institute for Meteorology,Germany (MPI-M) | × | ✔ | ✔ |

(precipitation, temperature, solar radiation, wind speed, relative humidity and air pressure) from the reference period (2006–2016) were considered. Three representative concentration pathways (RCP 2.6, RCP 4.5 and RCP 8.5, from low to high emissions) were analyzed in this study, along with historical simulations, in order to assess future snow and ice melt, mass balance change and runoff regimes. Note that the number of available simulations depends on the RCP (Table 1), and it is reduced from sixteen for RCP 8.5 and 4.5 to five for RCP 2.6.

Raw RCM data show systematic biases when compared with reference data. Thus, using raw RCM output without any post-processing for future impact modelling studies might lead to adaptation decisions based on incomplete information (Christensen et al., 2008). These biases are mainly associated with temporal and spatial disaggregation (Teutschbein and Seibert, 2012), inaccurate and incomplete representations of basic physical processes (Stevens and Bony, 2013) and parametrizations of unresolved sub-grid-scale processes such as precipitation, temperature inversion, cloud formation and convection. Such biases need to be minimized in order to reduce the bias they might induce in the evaluation of the impact on the hydro-climatological conditions of the area of interest. This can be achieved by using bias adjustment methods (establishing a correction factor between the historical simulation and the observations) or delta change methods.

In essence, the 'delta change' method consists in scaling (adding or multiplying) the observations by a change factor obtained from the comparison of two time slices in the model, e.g. future and historical (control) simulations. This way the temporal and spatial resolution of the reference observations is retained, thus an implicit downscaling is performed. A minimum number of years (e.g. 20) is preferably required for any climatological analysis (here, extracting the change factors), thus the control period must necessarily be longer than the observed data (2006 to 2016 only). Additionally, the typical control period in CMIP5 and CORDEX is 1986–2005 since historical simulations run up to 2005, which does not overlap the observations period. Therefore, the control period has been slightly shifted (1991–2010), but only for five years to avoid including RCP-forced simulations with evolving greenhouse gas emissions. In order to build this control period (1991–2010), data from the historical simulation (until 2005) were used together with data of the corresponding RCP4.5 simulation for each model for the remaining five years. Future projections are analyzed for two scenario periods (SCE) as near (2040–2059) and far future (2080–2099), to quantify snow and ice melt changes and runoff regimes over the Naltar catchment.

In this study, an improved form of the delta change method was applied at daily scale, by using an additive delta for temperature and air pressure as in Räisänen and Räty (2013) and a multiplicative correction factor for precipitation, relative humidity, wind speed and solar radiation (Räty et al., 2014). In the typical delta change approach, a climate change signal ("delta") is computed by comparing the raw climate model output for a future scenario period and the climate model output for a historical reference period. This delta is then used to scale observational time series in either an additive or a multiplicative manner, thus mean model biases are overlooked and the temporal structure of the new, projected time series follows the observed one. This method is a good alternative to bias correction when several variables are involved, since it preserves the inter-variable relationships in the reference data, at least for mean values at the time scale selected for the correction. However, one limitation of the method is the assumption of constant delta changes throughout the distribution. In order to account for varying deltas throughout the year, day-of-the-year (hereafter doy) dependent deltas can be used. Initially, the daily climatology (March-November) of each individual meteorological variable is computed for control (CTL) and (SCE) periods and each RCM separately and spectral smoothing (Bosshard et al., 2011), is used to reduce uncertainties and smooth the climatologies through a 31-day moving average.

In a second stage, additive (air temperature and pressure) and multiplicative (precipitation, relative humidity, solar radiation, wind speed) deltas were calculated for both SCE periods (2040–2059 and 2080–2099), relative to the CTL period (1991–2010). These change signals were used to project the observed meteorological time series to future scenarios in order to build climate change meteorological forcings, which are required at hourly temporal resolution to assess the glacio-hydrological response. The general equations for the improved delta method using both additive (Eq. (1)) and multiplicative (Eq. (2)) deltas which respect the bias in the mean and the changes in standard deviation of the scenario are given below:

$$X_{(h)}^{SCE,add} = \frac{\sigma_{SCE(d)}}{\sigma_{CTL(d)}}\left[X_{o(h)} - X_{CTL(d)}\right] + X_{SCE(d)} \quad (1)$$

$$X_{(h)}^{SCE,mult} = \frac{X_{SCE(d)}}{X_{CTL(d)}} X_{o(h)} \frac{\sigma_{SCE(d)}}{\sigma_{CTL(d)}} \quad (2)$$

where $X_{o\,(h)}$ indicates hourly meteorological observed series recorded at Naltar station, $X_{SCE(d)}$ and $X_{CTL(d)}$ denote the model 20-year mean for the day d (March-November) for the control and scenario periods, respectively, and $\sigma_{SCE(d)}$ and $\sigma_{CTL(d)}$ stand for the model 20-year standard deviation for the day d (March-November) for the control and scenario periods, respectively.

### 2.4. Energy and mass balance of snow and ice: The physically based hydrological model (PDSLIM)

In this section, the energy balance model, known as PDSLIM (Physically based Distributed Snow Land and Ice Model) is described. The PDSLIM model is the evolution of the PDSM model, applied at catchment scale to simulate snowmelt and snowpack dynamics in the Cordevole river first by Ranzi and Rosso (1991) and verified with in-situ passive microwave radiometry and snow gauging in Cagnati et al. (2004) and then applied to the debris-covered Belvedere glacier (Ranzi et al., 2004). Its soil-vegetation atmosphere exchange component adopts with a Penman Monteith scheme similar to that of Wigmosta et al. (1994) as developed first for the Toce catchment by Grossi and Falappi (2003) and then applied to the Adamello glacier by Ranzi et al. (2010) and Grossi et al. (2013), including heat and mass fluxes of glaciers partially covered by debris.

As described more in detail in Liaqat and Ranzi (2024) the annual glacier's mass balance is equal to the sum of winter and summer mass balances. It is assumed that winter starts on 1st of October of the previous year and ends on the 15th of March. The ablation season is assumed to start on the 16th of March of the given year, also considering a warm up period, and ends on the 30th of September of the balance year. The snow water equivalent at the beginning of the melt season can be considered the result of the winter glacier's mass balance, being computed as the sum of the snow mass balance and the firn and ice mass balance. The ice and firn winter mass balance is equivalent to the total volume of the snow water equivalent left at the beginning of the balance year, for us on the 1st of October, which starts its metamorphosis into firn and, later, ice. Ice melt is assumed to be negligible in winter. The snow winter balance, from the beginning of the accumulation year to the start of the melt season, is given by the difference between the snow water equivalent observed at the end and at the beginning of the winter season. Hence, the glacier's winter mass balance is given by the snow water equivalent at the beginning of the melt season and it is not necessary to simulate the accumulation and melt dynamics in winter, which could be also a difficult task because of the low quality of solid precipitation measurements in winter. In the control simulation in the current climate, snow water equivalent at the beginning of the melt season in each simulated year was derived from a combination of ground snow data and satellite data in Bair et al. (2016, 2020). The projected snowfall equivalent (SWE) for future simulations is calculated as the product of snow depth and snow density, assumed 300 kg/m$^3$ as in Liaqat and Ranzi (2024). The values of projected snow depth are

available in Table S6, which were obtained from the CORDEX-WAS44 and their associated ensembles for both future periods under the considered RCPs and were used to assess the winter mass balance in the future climate.The summer mass balance is computed from the melt assessed from the energy balance in the ablation season and the accumulation of solid precipitation. For a unit area, melt rate for finite depth of layer ice or snow superimposed over ice is computed using the energy balance equation:

$$H_m + H_c = S_{sn} + L_{ln} + H_l + H_s + H_p + H_g, \quad (3)$$

Here units of all terms are W/m$^2$. $H_m$: energy available for melt, $H_c$: internal energy of the snow or ice layer, $S_{sn}$: net shortwave radiation, $L_{ln}$: net longwave radiation, $H_l$: latent heat, $H_s$: sensible heat, $H_p$: advective heat from precipitation, $H_g$: conductive heat at the bottom of the snow or ice layer. The detailed description of the energy balance model in its snowpack, ice melt, radiative and turbulent fluxes components, can be found in the above mentioned papers as well as in the supplementary material. For projecting the glacier extent in the future, the literature suggests, for instance, the use of GloGEMflow model (Zekollari et al., 2019) which is the extended version of the Global Glacier Evolution Model GloGEM by Huss and Hock (2015) using multi model ensemble based climate forcings, mass balance and ice flow dynamics. In our approach the projected glacier extent was computed through an iterative procedure in which PDSLIM is run multiple times over a prescribed time period, while being forced by future meteorological scenarios and simulating glacier extent at each time step by preserving the computed mass balance in the changing climate. Initially, PDSLIM is run with present glacier boundaries and projected meteorological forcings for the near future (2040–2059) under RCP 4.5. The second step consists in computing the mean mass balance over a future period using the following formula:

$$MB_{2030} = (MB_{2010} + MB_{2050})/2 \quad (4)$$

Here $MB_{2010}$ is the mass balance of the eight simulated years according to the observations, $MB_{2050}$ refers to the mass balance in the near future (2040–2059) under RCP 4.5 and $MB_{2030}$ indicates the mean mass balance in current and future conditions. In the subsequent stage, it is assumed that the accumulation area, also known as the positive mass balance area, remains unchanged as the accumulated snow, which subsequently transforms into firn and then ice, flows through the glacier towards the ablation zone, which has a negative mass balance area. Accordingly, the mass balance in the ablation zone is rescaled to maintain the total glacier mass. The projected ice thickness $H_{ice,\ 2030}$, at the end of a twenty year period (2010–2030) is therefore computed using the following equation:

$$H_{ice,2030} = H_{ice,2010} - 20{*}MB_{2030}{*}\frac{Area_{total}{*}MB_{total}}{Area_{negative}{*}MB_{negative}}{*}\frac{1000}{917} \quad (5)$$

Here $H_{ice,2010}$ is the average ice thickness in meters at present, $Area_{total}$ is the total glacier's area in km$^2$, $Area_{negative}$ is the area of the ablation zone, $MB_{negative}$ represent the negative glacier's mass balance in the present conditions. The ratio 1000/917 is the ratio of water and ice density. Where the ice thickness results to be negative, because melting exceeds the ice flow redistribution from the accumulation zone, the ice extent is set to zero and is further incorporated into the bare rocks land use, in order to continue the iterative procedure for the further projection of mass balance and ice extent for 2050s, 2070s, 2090s time segment.

### 2.5. Projected water balance change using Turc-Budyko Theory

The projected water balance change in Naltar catchment was computed by Turc (1955) and Budyko et al. (1974) method. The Turc-Budyko plot was used to study the hydrological behaviour of the Naltar catchment particularly in terms of water balance for all selected RCMs and their multi-model ensemble mean in two future periods (2040–2059 and 2080–2099). The seasonal runoff coefficient or water yield ($Q/P$) was plotted as a function of seasonal long term aridity index ($P/ET_p$) (Coron et al., 2015).

$$Q/P = f(P/ET_p) \quad (6)$$

Here, $ET_p$, $Q$ and $P$ (mm) depict evapotranspiration, specific runoff and precipitation, respectively. If a relationship for a specific year lies above the water limit i.e. (Q > P) limit, it is referred to as glacier dominating catchment/ "Gaining zone". The Gaining zone (Q > P) indicates that there are additional water resources that contribute to net streamflow for glacierized catchments than just precipitation. Glacier and snow melt contribute to this additional water supply and the departure from the water limit line (Q = P) indicates how relevant is the contribution of glacier's and snow melt. Alternatively, a catchment is considered as a 'leaking catchment' when the runoff deficit P-Q is greater than the potential evapotranspiration, which means either precipitation is overestimated or some of the net runoff is not properly accounted for in the water balance, or water is stored in subsurface aquifers or surface storages as lakes, rivers and snowpack. However these additional storages in the absence of water artificial withdrawals or diversions are expected to be only temporary and on average their changes are expected to be negligible.

## 3. Results and Discussions

### 3.1. Simulation of snow and ice cover

The detailed description of the PDSLIM model outcomes for each simulated year to simulate snow and ice cover dynamics can be checked from Liaqat and Ranzi (2024). Overall snow and ice cover simulation indicates that the model slightly underestimates the spatial and temporal distribution of snow cover and ice areas compared to MODIS and LANDSAT (mean negative bias –1.8 %, NSE = 0.95, RMSE = 12.8 km$^2$ and $R^2$ = 0.96). As an example of the performance of the PDSLIM model during the reference period for the years 2012 and 2014, the comparison of simulated Snow Cover Areas (SCA) with LANDSAT and MODIS (M*D10A1GL06) based snow and ice cover map is shown in Fig.2 and Table 2.

### 3.2. Hydrological simulation

Simulated runoff computed by the linear reservoir lumped hydrological model (LRM) was compared with observed runoff on a daily basis during the melt season. The simulation resulted in average NSE 0.90 and 0.89 for the eight years of calibration and validation period respectively. The results of simulated streamflow for the years 2012 and 2014 along with a bar graph showing the amount of net precipitation are shown in Fig. 3.

Results show that the LRM model exhibited satisfactory performance while simulating hydrological components with a $R^2$, NSE and KGE of 0.85, 0.83 and 0.83 and 0.95, 0.94, 0.91, respectively, during the 2012 and 2014 year. A more detailed analysis of observed and simulated runoff during the calibration and validation period can be found in Liaqat and Ranzi (2024).

These findings indicate that the PDSLIM and LRM modeling framework is capable of reproducing snow and ice melt and the routed runoff and, reasonably, that it can be used to project hydro-glaciological regimes in the Karakoram in the future climate as well.

### 3.3. Future climate change signals

Results in Fig. 4 show the change signals for the scenario period (2040–2059 and 2080–2099) relative to the control period (1991–2010) using sixteen CORDEX-WAS44 simulations for the grid box over the

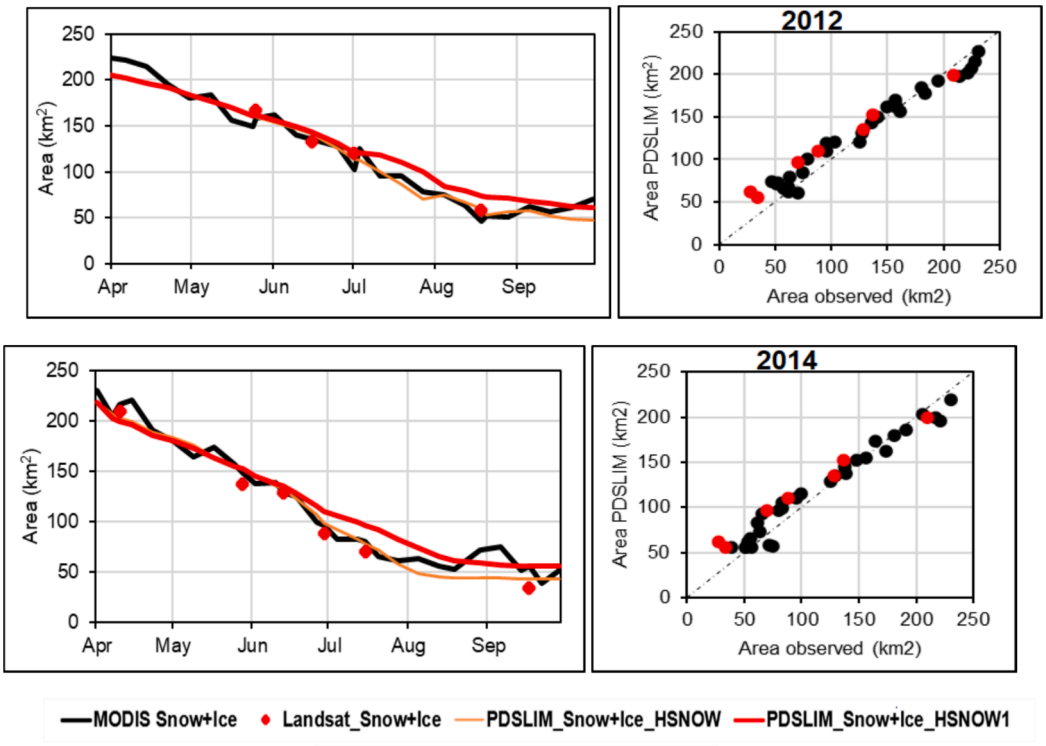


**Fig. 2.** Comparison of MODIS (M*D10A1GL06) and LANDSAT with simulated snow cover area (2012, 2014) with Temperature Lapse Rate (−0.0065 °C $m^{-1}$ and −0.0051 °C $m^{-1}$) for clear sky and cloud cover. Here HSNOW refers to snow depth derived from MODSCAG based SWE and HSNOW1 refers to snow depth derived SPIRES based SWE.

**Table 2**
Statistics evaluation of snow and ice cover simulation for 2006–2016.

| Year | NSE | MaxE ($km^2$) | Bias % | MAPE (%) | RMSE ($km^2$) | $R^2$ |
|---|---|---|---|---|---|---|
| 2006 | 0.93 | 20.5 | −2.3 | 13.0 | 14.1 | 0.93 |
| 2008 | 0.97 | 2.5 | −2.1 | 8.3 | 9.0 | 0.98 |
| 2009 | 0.96 | 19.9 | 0.5 | 9.1 | 11.5 | 0.97 |
| 2010 | 0.91 | 16.8 | 2.4 | 9.8 | 15.9 | 0.96 |
| 2011 | 0.94 | 19.8 | −2.0 | 12.9 | 13.2 | 0.95 |
| 2012 | 0.94 | 13.1 | −4.8 | 14.0 | 14.1 | 0.97 |
| 2014 | 0.95 | 2.1 | −3.0 | 12.5 | 12.9 | 0.96 |
| 2016 | 0.96 | 19.8 | −3.3 | 13.0 | 11.4 | 0.97 |
| Average | 0.95 | 14.3 | −1.8 | 11.6 | 12.8 | 0.96 |

Naltar catchment under three RCPs 2.6, 4.5 and 8.5. The study is focused on the months from April to September in order to examine the melting and monsoon season, when a large fraction of streamflow is generated. The ranges of the mean projected changes and the projected changes in terms of standard deviation were examined and served to detect outliers which might lead to undesired effects in the hydrological projections. Additive and multiplicative climate change signals for both mean values and their standard deviation precipitation, relative humidity, wind speed, solar radiation, temperature and air pressure are shown in Fig.4 and Fig.S1.

For precipitation, multiplicative delta changes vary largely across models during the summer season, especially for RCM11, RCM12,

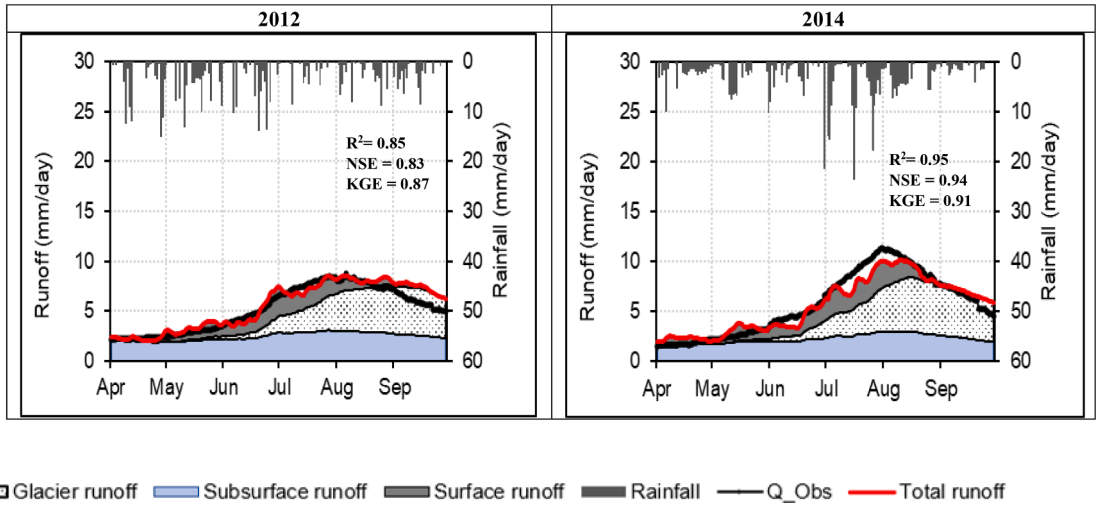


**Fig. 3.** Comparison of observed and simulated runoff at Naltar Bala (Naltar Catchment outlet) during 2012 and 2014 with rainfall; seasonal distribution of mean monthly flow composition (Baseflow, Glacier runoff, Subsurface runoff, and Surface runoff).

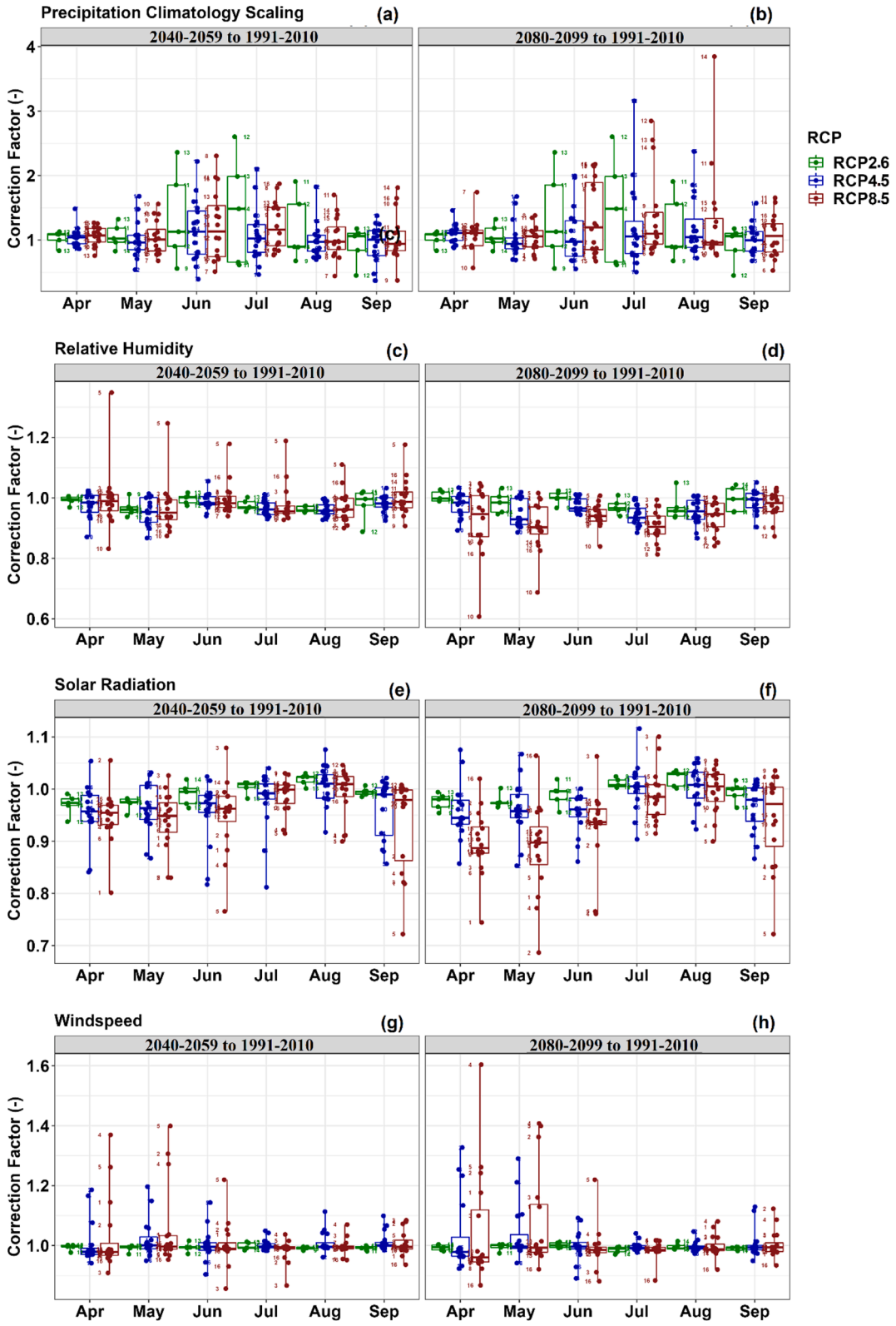


**Fig. 4.** Melting cycle (April-September) of multiplicative (unitless) change factors for precipitation, relative humidity, solar radiation, wind speed and additive change factors for temperature (°C) and air pressure (hPa) over the scenario periods (2040–2059 and 2080–2099) relative to the control period (1991–2010) for the 16 CORDEX-WAS44 simulations (individual numbered dots within the boxes, see Table 1) under 3 RCPs (colours). The change factors were obtained for each doy from the daily annual cycle in the scenario and control periods (see Methodology) and were here averaged into monthly values.

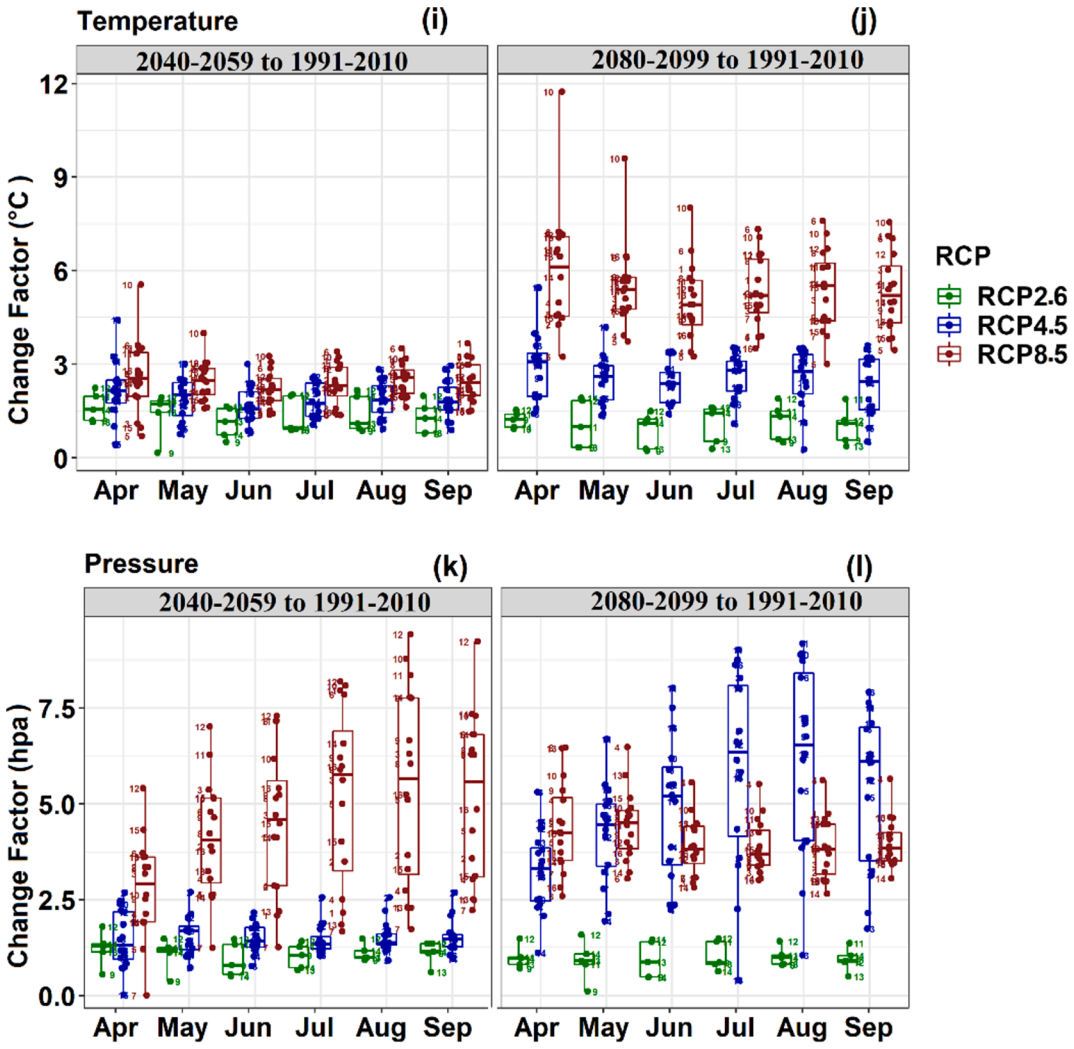


**Fig. 4.** (*continued*).

RCM13, RCM14, RCM15, for both mean values (Fig. 4, panels a,b) and their standard deviation (Fig.S1, panels a,b) under RCP 4.5 and 8.5. RCP 2.6, for which five simulations are available, RCMs 11, 12, 13 present larger deviations (and even the largest changes among scenarios for the near future period). Considering the three RCPs, change factors (as ratios) of all RCMs range between 0.37 and 2.60 and 0.45 – 3.85 for mean precipitation and 0.33 – 3.60 and 0.34 – 6.24 for its standard deviation during near future and far future periods, respectively. According to the IPCC Interactive Atlas (Gutiérrez et al. 2021; Iturbide et al. 2022), the projected increase in precipitation using different (regional and global) model ensembles in this region is between 25–35 % by the end of the 21st century, which is in line with previous literature (Azmat et al., 2020; Jury et al., 2020). According to our results, the largest values (above 2, i.e. more than doubling mean precipitation and its variability on monthly time scales) occur for June-August in 2080–2099 and always for specific models, thus they were considered unrealistic and excluded from subsequent analyses. Note that change factors depicted in the figure are monthly averages for visualization purposes, but change factors are applied on a daily basis (see Sec. 2.3), thus with greater variability. Such large factors imply increases in precipitation of up to 52 % when applied to the reference data (following Eq. (2), which would mean a large overestimation which is not coherent with the sources cited above. Model selection is not an easy task, and it is commonly based on data availability by Fatima et al. (2020) or model performance compared to observations (Azmat et al., 2020). Yet, considering model performance, it is difficult to separate between 'good' and 'bad' models, since their ability to represent the observed climate usually depends on the considered metric and because the whole process of model development, evaluation, and posterior weighting or ranking typically use the same reference datasets (Knutti et al., 2010). Overall, the models' ability to simulate present-day climate conditions is weakly associated with the magnitude of the predicted change by Knutti et al. (2010) and, although agreement between model and observations is desired, it is not a sufficient condition for their credibility (Oreskes et al., 1994). Hence, another important factor to consider is models' plausibility and future spread in order to represent credible future changes (Sobolowski et al., 2023, Katragkou et al., 2024). Considering these issues and the results for models with unrealistic projected changes, they were excluded from all meteorological variables for the subsequent hydrological simulation. If we exclude from the final ensemble the above-mentioned five RCMs (namely RCM11, RCM12, RCM13, RCM14, RCM15), the projected increase in precipitation lies around 29 % by the end of this century under RCP 8.5, according to the ensemble mean.

An increase in temperature was found for both future periods under RCP 4.5 and RCP 8.5 (Fig. 4, panels i, j, Fig. S1, panels i, j), especially towards the end of the century (2080–2099) under RCP 8.5. It is also observed that a substantial rise in the change signal and standard deviation for temperature is more accentuated during the pre-monsoon (April-May) especially for 2080–2099 under RCP 8.5. Similarly, the rising delta change of temperature is also prominent during the

monsoon (June-September) with temperature changes ranging between +1.7 °C to +5.4 °C. Overall, monthly mean temperature change factors show an important increase in temperatures from present to far future period and vary largely across all considered RCPs, since they span from +0.87 °C to +6.02 °C in both future periods. The rise in temperature and precipitation changes of the current study are in line with present climate trends shown in previous field campaigns (Ali et al., 2015; Soncini et al., 2015; Kraaijenbrink et al., 2017; Jury et al., 2020).

For relative humidity (RH), overall, small delta changes were found in both the mean and the standard deviation as shown in (Fig.4, panels c, d). It is also observed that a couple of outlier simulations leads to a larger delta change in the near future (RCM5) and smaller in the far future (RCM10), respectively. Change factors for all RCMs range between 0.83 and 1.35 and 0.61 – 1.1 (as multiplicative ratios) for mean relative humidity and 0.9 – 2.1 and 0.9 – 1.7 for its standard deviation (Figs. S1, panels c,d) during the near future and far future periods, respectively. For solar radiation, marginal change factors were found for RCP 2.6. However, signals get larger from near future to far future under RCPs 4.5 and 8.5 especially in April and May as a consequence of the projected global warming in this region, under RCPs 4.5 and 8.5 (Fig.4, panels e, f). The range of the monthly mean change factors for all RCMs is 0.8 – 1.4 and 0.9 –1.6 (as ratios) for solar radiation and 0.9 – 2.1 and 0.9 –1.7 for its standard deviation (Fig. S1, panels e, f), considering all RCPs for both periods. Wind speed is also an important component of energy balance and hydrological modeling studies. Overall, the climate change simulations revealed small changes in this variable, with some indication of future increase towards the end of the century. This increase is larger in the pre-monsoon season than in summer in terms of mean wind speed (Fig.4, panels g, h).. Such differences can be linked with early snow melt especially in glacierized catchments (Shakoor and Ejaz, 2019). Similarly, the increase in monthly mean change factors for wind speed is larger for RCP 8.5 compared to RCP 4.5, while RCP 2.6 did not exhibit important changes, both in terms of mean and standard deviation. Change factors for 16 RCMs range between 0.72 and 1.08 and 0.69 – 1.1(as ratios) for the mean wind speed and 0.75 – 1.55 and 0.64 – 1.87 for standard deviation during the near future and far future period, respectively. For air pressure, a small increasing delta change (less than 10 hPa) is projected both in terms of the mean (Figs. 4, panels k, l) and standard deviation (Fig. S1, panels k, l), especially for RCP 8.5 for near future and RCP 4.5 and 8.5 for far future.

Overall, it is found that delta changes for temperature and precipitation exhibited large spread among RCMs, scenarios and periods both in terms of the mean and of the variability, while other variables depict more robust and smaller changes. Temperature and precipitation have a crucial role in hydrological and mass balance studies. Note that the exclusion of five RCM11-RCM15) from the final model ensemble led to a reduction of the unexpected and too remarkable overestimation in terms of precipitation increase. Therefore, they were excluded from all meteorological variables for the subsequent hydrological simulations. By doing so, the final size of the model ensemble is eleven simulations for RCP 4.5 and RCP 8.5 but only one for RCP 2.6.

### 3.4. Projected changes in snow water equivalent

The projected rise of temperature in the Naltar catchment is expected to have substantial implications for snow water equivalent (SWE), snow melt and runoff regimes. The projected changes of SWE available at the beginning of the melting season for both scenario periods and considered RCPs are provided in Table 3. Winter mass balance was not modelled, but was assumed based on the SWE at the beginning of the melt season (rescaled from snow depth given by the climate models). The PDSLIM simulations indicate that at present conditions (average over the eight years within 2006–2016), the average snow water equivalent in Naltar catchment which is available for melt is 1465 mm. The SWE proportion is projected to decrease to 1332 mm (– 9.1 % less) and 1184 mm (−19.2 % less) according to the multi-model ensemble mean in near future (2040–2059) under RCP 4.5 and RCP 8.5, respectively. Additionally, by the far future (2080–2099), the proportion of SWE will reduce to –6.1 % less and –37.4 % less under RCP4.5 and RCP8.5, respectively. For RCP 2.6 (only one RCM9), projected SWE shows an increasing SWE (+21.2 %) in near future and decreasing rate (−17.2 %) in the far future. The overall projections from PDSLIM simulations indicate a substantial decline in the multi-model ensemble SWE at the onset of the melting season when compared to the present climate, for both the scenario periods and under the RCPs (4.5 and 8.5). This reduction in SWE at the start of the melting season leads a more rapid melting of snow, resulting in the early exposure of the glacier's surface, and subsequently accelerates the melting of glaciers due to decrease albedo. These results are in line with previous studies (Lutz et al., 2016; Romshoo and Marazi, 2022) who found significant changes in the form of precipitation and SWE in the Indus and Jehlum basin.

**Table 3**
Projected changes in snow water equivalent available for melt at the beginning of April for each RCM in both future time periods relative to present climate 2006–2016 under RCP 2.6 (for RCM 9 only), RCP 4.5 and RCP 8.5. "Ensemble" refers to the mean value of all individual simulations for each RCP.

| | | 2040–2059 | | 2080–2099 | |
|---|---|---|---|---|---|
| | | mm | Change (%) | mm | Change (%) |
| | Reference | 1465 | | 1465 | |
| **RCP26** | *RCM9* | *1775* | *21.2* | *1213* | *−17.2* |
| **RCP45** | RCM1 | 1332 | −15.5 | 1376 | −6.1 |
| | RCM2 | 1332 | −15.5 | 1376 | −6.1 |
| | RCM3 | 1332 | −15.5 | 1376 | −6.1 |
| | RCM4 | 1332 | −9.1 | 1376 | −8.4 |
| | RCM5 | 1332 | −9.1 | 1376 | −6.1 |
| | RCM6 | 1095 | −25.3 | 1302 | −11.1 |
| | RCM7 | 1790 | 22.2 | 1775 | 21.2 |
| | RCM8 | 1612 | 10.1 | 1494 | 2.0 |
| | *RCM9* | *1553* | *6.0* | *1435* | *−2.0* |
| | RCM10 | 681 | −53.5 | 1583 | 8.0 |
| | RCM16 | 1332 | −9.1 | 1376 | −6.1 |
| | **Ensemble** | **1332** | **−9.1** | **1376** | **−6.1** |
| **RCP85** | RCM1 | 1184 | −24.9 | 918 | −37.4 |
| | RCM2 | 1184 | −24.9 | 918 | −37.4 |
| | RCM3 | 1184 | −24.9 | 918 | −37.4 |
| | RCM4 | 1184 | −19.2 | 918 | −37.4 |
| | RCM5 | 1184 | −19.2 | 918 | −37.4 |
| | RCM6 | 844 | −42.4 | 696 | −52.5 |
| | RCM7 | 1627 | 11.1 | 1435 | −2.0 |
| | RCM8 | 932 | −36.4 | 1036 | −29.3 |
| | *RCM9* | *1479* | *1.0* | *1154* | *−21.2* |
| | RCM10 | 932 | −36.4 | 282 | −80.8 |
| | RCM16 | 1184 | −19.2 | 918 | −37.4 |
| | **Ensemble** | **1184** | **−19.2** | **918** | **−37.4** |

### 3.5. Projected change in snow and ice melt dynamics and mass balance

The projected snow and ice cover area according to the individual RCMs and the multi-model ensemble mean under three RCPs (2.6, 4.5 and 8.5) is shown in Fig.5. The primary reason to develop snow and ice melt time series is using individual models is to examine the spread in glacio-hydrological projections, especially during the years of flood occurrence, which is sometimes neglected when using the ensemble of all simulated models. For RCP 2.6 (only one RCM available, RCM9), results indicate increasing snow and ice melting shrinkage (–25.9 %) in the near future (2040–2059) and –51.5 % in far future (2080–2099) relative to present climate.

For RCP 4.5 and RCP 8.5, almost all RCMs and the ensemble means exhibit gradual increase in snow followed by ice melt. It is also noticed that the relative change in snow and ice melt time series produced by each RCM is different from each other and that the spread of results is very high with RCP 8.5. Under RCP 4.5, snow and ice melt depletes further in the ranges from –5.4 % to –56.3 % (ensemble mean –36.5 %) in the near future (2040–2059) and depletes further up to –30.4 % to

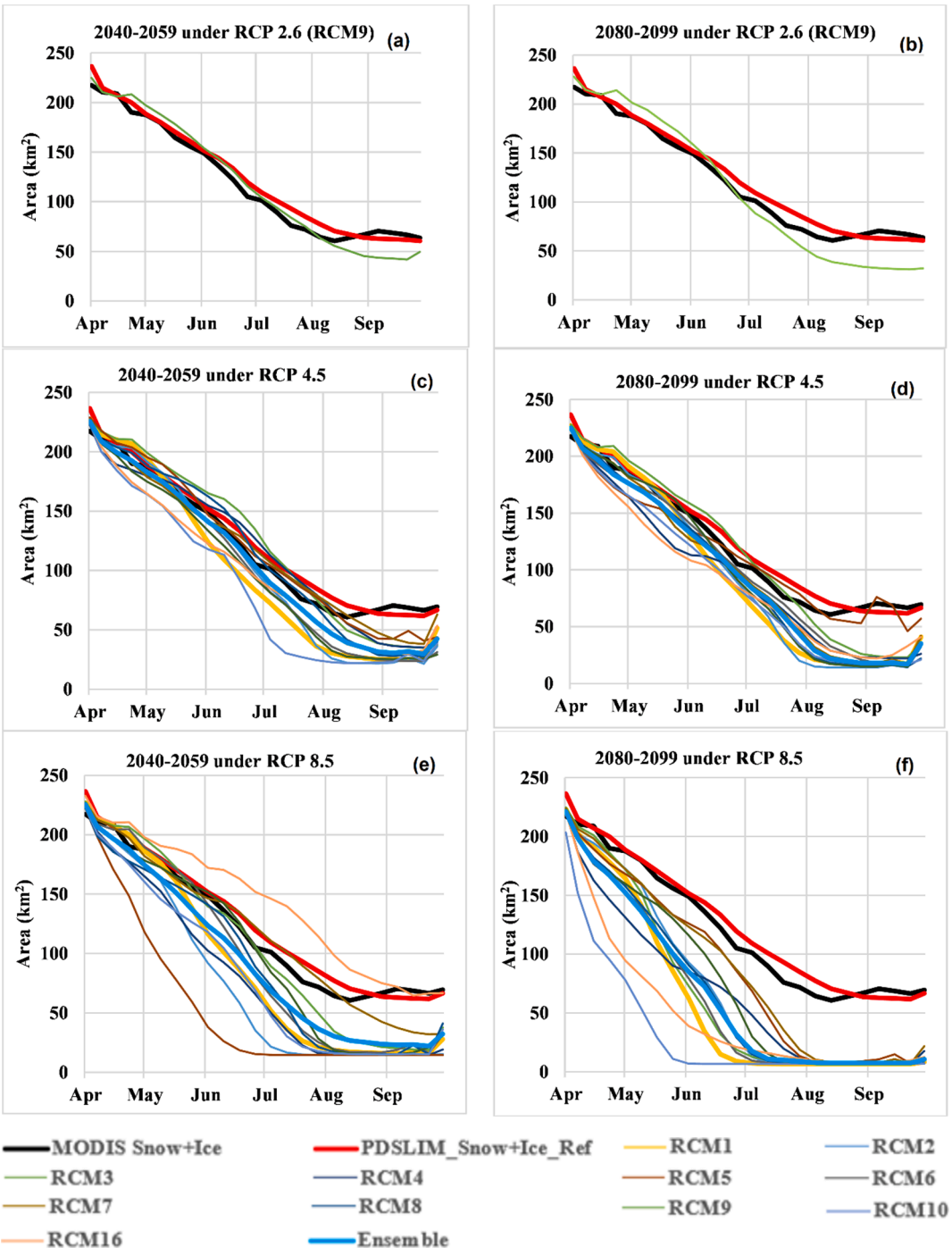


**Fig. 5.** Future annual cycle (April to September) of snow and ice melt progression over the Naltar catchment according to different CORDEX simulations (coloured lines) and their multi-model ensemble mean (thick blue line) for near future (2040–2059) and far future (2080–2099) for RCPs (2.6, 4.5, 8.5). MODIS (black line) and PDSLIM simulation (thick red) in the reference period (8 years) are shown for reference.

–67.9 % (ensemble mean –47.7 %) by the end of the century. The higher projected increase in snow and ice melt is mostly linked with higher temperature. Under RCP 8.5, rapid snow and ice melt depletion is projected with snow cover completely disappearing by mid of June followed by ice melt in early July. The projected change in snow cover area (SCA) ranges from 0.2 % to –78.2 % (ensemble mean –51.5 %) during near future (2040–2059) and depleted further in the range –67.4 % to –87.6 % (ensemble mean –83 %) in the far future (2080–2099) under RCP 4.5 and RCP 8.5 respectively.

The largest increase by the end of the century is found for the transitional months (May and June), when a larger part of precipitation is projected to fall into liquid form in the future followed by earlier ice melt in July (for RCP 4.5) and in June instead of in July for RCP 8.5 by the end of the century (Fig.9). Early seasonal snow and ice melt enhance risk of increased flooding and landslides because of the rapid melt. As one example, a glacial surge occurred in the Upper Naltar valley on July 5, 2021. There were four fatalities, over 150 livestock killed, and 4 km of pastureland was destroyed by the avalanche (Dawn, 2021). The reduced snow precipitation during the accumulation period and rapid melting of the depleted snow also led to the early exposure of the glacier surfaces thus enhancing the melting of glaciers in the catchment.

### 3.6. Glacier mass change projections

To estimate the response of the Naltar glaciers to future climate forcings, the calibrated PDSLIM model was employed to project annual mass balance for all individual glaciers with an area larger than 0.4 $km^2$. This is done by assessing, first, the future winter mass balance assessed from rescaling the end-of-winter SWE estimated by Bear et al. (2016, 2020) with the snow depth model projections as given in Table S6 and the future summer mass balance simulated with PDSLIM in both future periods. Moreover, projected simulations using an ensemble of RCMs also translated into projected change in glacier extent and mass balance given in Table 4.

Overall results of Table 4 indicate that glaciers are already in conditions of negative mass balance in the Naltar catchment with reference value of −737 mm w.e. $a^{-1}$ in today's climates (Fig.6 and Table S5). Projections estimate that from 2010 to 2100, glaciers in the Naltar catchment will vary their mean mass balance (with annual mass losses ranging from –654 to –1621 mm w.e. $a^{-1}$ by 2040–2059 and 2080–2099 respectively) in the two future periods under RCP 2.6 with RCM9. Worth to note the fact that the projected annual mass balance in the near future under RCP 2.6 is a little less negative than in the reference period because the increased SWE at the beginning of the melt season (1775 vs. 1465 mm in Table 3) compensates for the increased summer melt. For RCP4.5, mass balance range between +128 to –2436 mm w.e. $a^{-1}$ with ensemble mean of –887 mm w.e. $a^{-1}$ in the near future (2040–2059) and –352 to –2277 mm w.e. $a^{-1}$ with ensemble mean –1154 mm w.e. $a^{-1}$ in the far future scenario (2080–2099), as shown in Table S5. For RCP8.5, mass balance varies between +1197 to –6913 mm w.e. $a^{-1}$ with ensemble mean –2018 mm w.e. $a^{-1}$ in the near future (2040–2059) and from –1508 to –4489 mm w.e. $a^{-1}$ with ensemble mean –2597 mm w.e. $a^{-1}$ in the far future scenario (2080–2099). The spatial variability in projected mass loss is dependent on the projected temperature, precipitation, present-day mass balance and several glacier attributes such as, e.g., ice thickness and glacier hypsometry. Overall, a rise in temperature varies between 0.87 °C to 6.02 °C in both future periods during both scenario periods under all RCPs. Although, multi-model ensemble mean of total precipitation (April-September) is also projected to increase by 29.4 % under RCP 8.5 by the far future period (Sec. 3.3), it cannot compensate for the substantial increase in temperature.

Such projected changes in temperature will accelerate snow and ice melt and will eventually reduce ice volumes from –27 % to –80 % and change negative glacier mean annual mass balance between –654 to –2597 mm w.e. $a^{-1}$ under different future periods, as shown in Table 3. Worth to note is that the annual mass balance by the near future is expected to become less negative than in the reference period (–654 mm instead of –737 mm) because of the projected increase of the winter mass balance (1775 mm vs. 1465 mm) resulting from increased projected snow depth. Results show that glacier extent in the Naltar catchment is projected to lose –27 % to –43 % under RCP 2.6, –41 % to –60 % under the RCP 4.5, and –58 % to –80 % under the RCP 8.5 relative to present extent (Fig. 7).

**Table 4**
Projected annual mass balance and ice extent for 2050 and 2090 relative to reference period 2006–2016 in the Naltar catchment. Individual RCMs' results are shown in Table S5.

| Mass balance scenario | Average (mm w. e. $a^{-1}$) | Ice extent ($km^2$) | Change (%) |
|---|---|---|---|
| Reference Period (Average for 8 years) | –737 | 36.17 | |
| 2040–2059 under RCP 2.6 (RCM9) | –654 | 26.40 | −27 % |
| 2040–2059 under RCP 4.5 | –887 | 21.50 | −41 % |
| 2040–2059 under RCP 8.5 | –2018 | 15.10 | −58 % |
| 2080–2099 under RCP 2.6 (RCM9) | –1621 | 20.60 | −43 % |
| 2080–2099 under RCP 4.5 | –1154 | 14.50 | −60 % |
| 2080–2099 under RCP 8.5 | –2597 | 7.40 | −80 % |

Our findings are in agreement with Rounce et al. (2020) who projected glacier mass change in High Mountain Asia using the PyGEM model by employing data of 22 GCMs and four RCPs. Overall, their results show that the retreat of glaciers in the Naltar catchment varies considering uncertainties between –35 % to –71 %.

We found a mass loss in the Naltar catchment that is 5–10 % higher than in previous studies under considered RCPs. Such differences in glacier projections are possibly due to the use of different climate forcings (GCM and RCP scenarios), climate spread with diverse range of RCMs, model physics, observed meteorological data and calibration scheme, present day mass balance and various glacier attributes (e.g., ice thickness and glacier hypsometry). Rounce et al. (2020) also mentioned that PyGEM is presently designed for large scale applications and its model physics allows instant estimations over large catchments (e.g., use of mass distribution curves). Care should be taken when applying this model especially at small scales, while PDSLIM is suitable for small scale and high resolutions applications. Moreover, Kraaijenbrink et al. (2017) also found that the regional variation in mass loss in High Mountain Asia (HMA) is quite large and there are several regions where the ice mass and glacier area is less than 10 % under RCP 8.5 compared to present conditions. Hence, these arguments strengthened our results about higher specific mass loss and glacier area retreat as compared to other parts of HMA where the so-called 'Karakoram anomaly' prevails. As a result of these projections, regional water management and mountain communities may experience serious consequences. The results of our study also show that the Karakoram anomaly has less impact especially at this small-scale catchment in the southern region of Karakoram. Future work should seek to continue the use of physical models for future mass balance and glacier retreat studies and to explore the Karakoram anomaly in the context of climate change in glacierized catchments as well as glacier outburst regions in Pakistan.

### 3.7. Projected change in streamflow

In order to predict the impact of climate change on future streamflow during melting season, from April to September, the linear reservoir model already calibrated and validated by Liaqat and Ranzi (2024) was run with future climate forcings. The hydrological model parameters were kept the same during future simulation. The predicted streamflow hydrographs for two future scenario periods 2040–2059 and 2080–2099 under three RCPs 2.6, 4.5 and 8.5 are shown in Fig.8. The uncertainty in the future climate of Naltar catchment is also evident in projections of future hydrology. Results show different projected temporal variability in streamflow in all selected climate models under three RCPs in the Naltar catchment. Under RCP 2.6 with RCM9, the projected streamflow is found to be increasing in magnitude (June-August) in the near future followed by steady decline (July-September) during the far future period. It is also seen in Fig.8. that peak streamflow is shifted from Aug-Sep to June-July by the end of the century in both future periods, respectively.

Under RCP 4.5, projected streamflow exhibits increases and decreases with respect to reference period in both future scenarios for the different RCMs. Overall, the multi-model ensemble mean projected streamflow is expected to follow a slight decrease to 942 mm in near future 2040–2059 following the steady 993 mm in the far future 2080–2099. The peak runoff curve is also shifted from August-September to July-August by the end of the century. Under RCP 8.5, the projected streamflow is expected to continuously decrease 931 mm in the near future 2040–2059 and 733 mm in the far future 2080–2099 compared to the reference 960 mm as shown in Table 7.

Fatima et al. (2020) argued that peak flow timings in the Hunza basin will remain unchanged in the near future (2037–2066) while peak flow changes in timing will become more pronounced under RCP 8.5 in the far future (2067–2096), with a slight early onset. Azmat et al. (2020) also examined inter-annual changes in peak streamflow in the Hunza

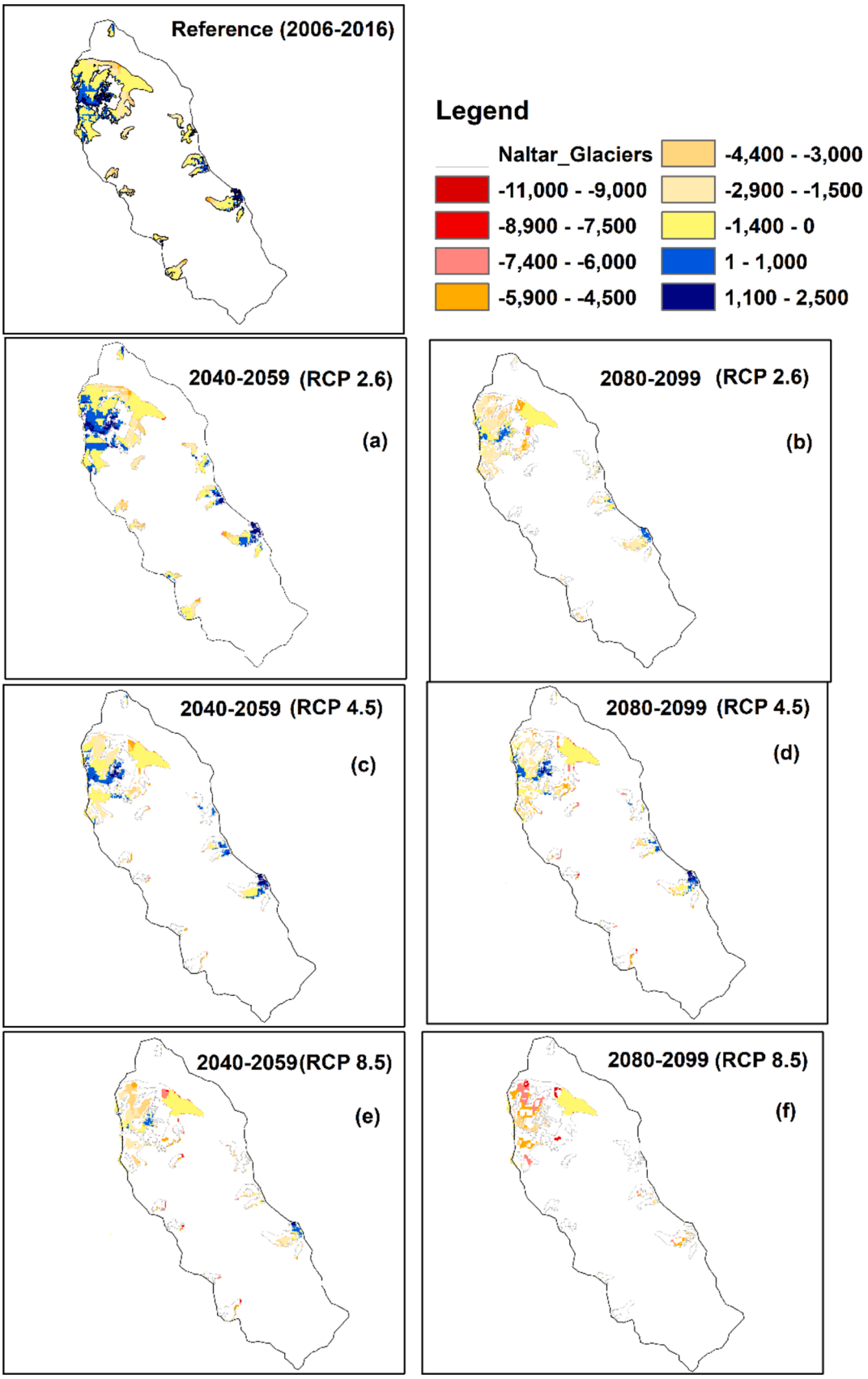


**Fig. 6.** Observed (upper left panel) and projected glacier mass loss (mm w.e. $a^{-1}$) for the multi-model ensemble mean of the PDSLIM simulations driven by the CORDEX RCMs for 2040–2059 and 2080–2099 (columns) and RCP 2.6, RCP 4.5 and RCP 8.5 (rows).

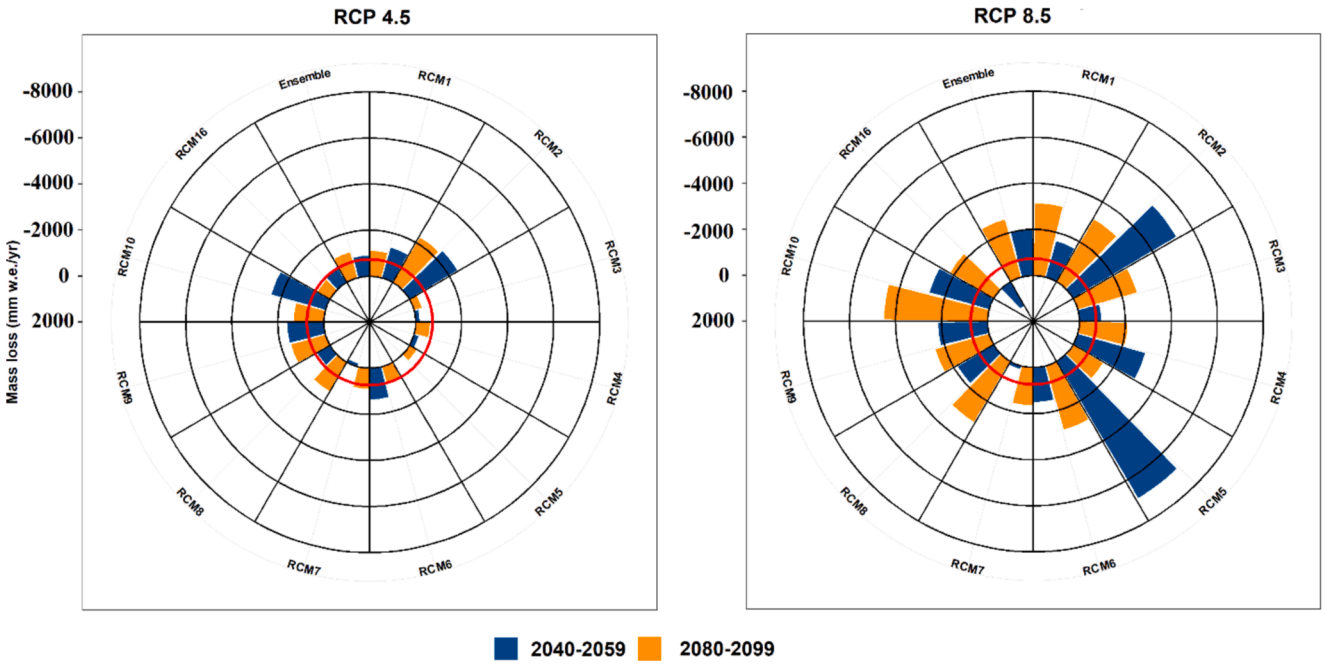


**Fig. 7.** Projected changes in mass balance loss over the Naltar catchment for the individual CORDEX simulations and multi-model ensemble for near future (2040–2059) and far future (2080–2099) periods for two RCPs (4.5, 8.5). The red line depicts the observed mass loss in 2010–2016 (−737 mm w.e. $a^{-1}$).

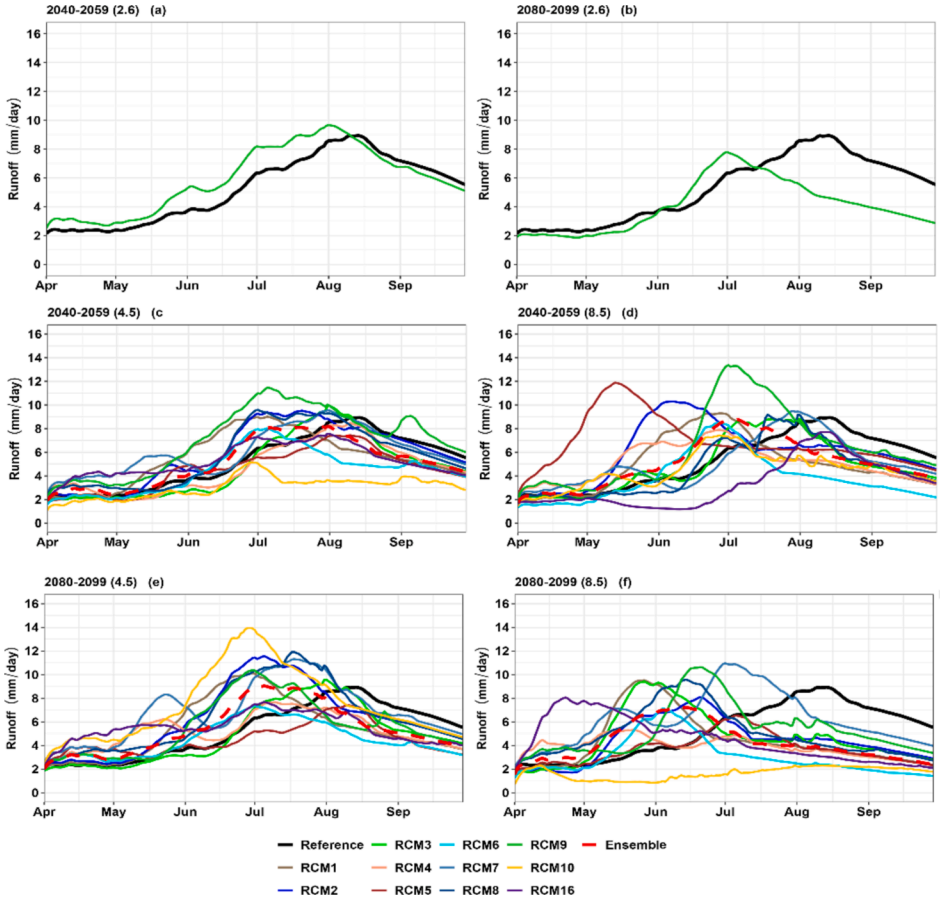


**Fig. 8.** Daily runoff simulated for the observed period (2006–2016) and projected runoff of scenario years (2040–2059 & 2080–2099) under RCP 2.6, RCP 4.5 and RCP 8.5 of the Naltar catchment.

and neighboring basins using four CORDEX-WAS44 RCMs and their ensemble mean. Their results revealed a sharp increase in streamflow during the pre-monsoon season, followed by a subsequent decline during the monsoon season. They also found a one-month earlier shift in streamflow during both the pre-monsoon snowmelt period (April to June) and monsoon (July to September) seasons during the 2090 s. The outcomes of our research on peak flow timing for the majority of RCMs and their ensemble mean exhibit substantial shifts from August-September to mid of June to July in the near future (2040–2059) whereas to mid of May to the end of June in the far future (2080–2099). These significant changes in streamflow dynamics exhibit some variability linked to the diverse RCMs we explored in our research, thus providing an assessment on the uncertainty introduced by the large climate projections spread resulting from the choice of models.

Table 5 illustrates the projected monthly and mean seasonal variation in streamflow and its change under the three RCPs (2.6, 4.5, 8.5) for each selected model and the multi-model ensemble mean. Overall, we found that the mean seasonal streamflow increased under RCP 4.5 in both future periods. Under RCP 8.5, mean seasonal streamflow also increases in the near future (2040–2059), but declines in the far future.

**Table 5**
Naltar monthly streamflow percentage changes by individual CORDEX climate models and their ensemble mean under RCP 2.6, RCP 4.5 and RCP 8.5 as compared to reference period.

| RCM | RCP | Decade | Apr | May | Jun | Jul | Aug | Sep | Mean |
|---|---|---|---|---|---|---|---|---|---|
| RCM1 | RCP45 | 2050s | 1.2 | 45.7 | 66.9 | 16.6 | -24.4 | -23.2 | 13.8 |
| | | 2090s | 3.2 | 33.0 | 97.8 | 15.0 | -35.5 | -34.2 | 13.2 |
| | RCP85 | 2050s | -1.6 | 54.3 | 78.6 | -4.3 | -39.9 | -40.5 | 7.8 |
| | | 2090s | -4.3 | 142.3 | 46.0 | -47.6 | -65.7 | -66.6 | 0.7 |
| RCM2 | RCP45 | 2050s | 6.3 | 23.0 | 33.0 | 31.1 | -2.3 | -2.4 | 14.8 |
| | | 2090s | 10.1 | 29.5 | 88.0 | 47.9 | -17.4 | -16.7 | 23.6 |
| | RCP85 | 2050s | 10.6 | 94.9 | 96.4 | -0.2 | -18.5 | -13.8 | 28.2 |
| | | 2090s | -20.4 | 63.3 | 64.0 | -35.9 | -57.3 | -58.6 | -7.5 |
| RCM3 | RCP45 | 2050s | -3.0 | -22.2 | -30.3 | 21.1 | -3.5 | -20.2 | -9.7 |
| | | 2090s | -5.8 | -10.3 | -5.7 | 18.0 | -10.0 | -26.0 | -6.7 |
| | RCP85 | 2050s | 0.2 | 11.0 | -0.9 | 35.6 | -20.2 | -28.8 | -0.5 |
| | | 2090s | -16.5 | 122.2 | 68.0 | -40.9 | -55.3 | -57.6 | 3.3 |
| RCM4 | RCP45 | 2050s | 19.6 | -19.4 | -17.6 | -3.4 | -9.2 | -21.2 | -8.5 |
| | | 2090s | 38.0 | 86.0 | 13.5 | 4.2 | -27.4 | -33.9 | 13.4 |
| | RCP85 | 2050s | 34.0 | 83.4 | 59.2 | -14.2 | -39.3 | -40.2 | 13.8 |
| | | 2090s | 60.4 | 68.9 | -7.0 | -40.9 | -64.8 | -65.6 | -8.2 |
| RCM5 | RCP45 | 2050s | -6.3 | 1.4 | 7.2 | -14.2 | -18.9 | -29.0 | -10.0 |
| | | 2090s | 47.8 | 15.7 | -8.0 | -21.0 | -21.8 | -40.4 | -4.6 |
| | RCP85 | 2050s | 127.9 | 264.4 | 64.5 | -10.5 | -26.6 | -20.0 | 66.6 |
| | | 2090s | -1.4 | 12.6 | 3.0 | -22.1 | -61.9 | -62.8 | -22.1 |
| RCM6 | RCP45 | 2050s | -7.5 | -10.8 | 25.1 | -0.5 | -40.2 | -28.4 | -10.4 |
| | | 2090s | 25.0 | 8.0 | 31.0 | -6.2 | -42.9 | -41.4 | -4.4 |
| | RCP85 | 2050s | -32.3 | -7.8 | 48.0 | -19.6 | -55.9 | -57.9 | -20.9 |
| | | 2090s | -14.6 | 39.2 | 24.0 | -63.7 | -80.4 | -85.5 | -30.2 |
| RCM7 | RCP45 | 2050s | 58.4 | 77.4 | 9.7 | 19.7 | -1.1 | -9.6 | 25.7 |
| | | 2090s | 54.3 | 122.0 | 47.7 | 52.0 | -4.5 | -9.9 | 43.6 |
| | RCP85 | 2050s | 24.9 | 43.9 | -17.1 | 10.2 | -10.6 | -26.6 | 4.1 |
| | | 2090s | 48.1 | 114.9 | 64.1 | 38.0 | -31.7 | -34.7 | 33.1 |
| RCM8 | RCP45 | 2050s | 30.3 | -0.5 | 35.5 | 29.4 | -7.0 | -14.1 | 12.3 |
| | | 2090s | 37.9 | 34.0 | 71.3 | 54.8 | -9.2 | -17.1 | 28.6 |
| | RCP85 | 2050s | -4.5 | -16.2 | 2.7 | 9.0 | -21.1 | -33.4 | -10.6 |
| | | 2090s | 38.3 | 91.6 | 96.2 | -31.3 | -61.4 | -61.3 | 12.0 |
| RCM9 | RCP26 | 2050s | 25.3 | 25.6 | 33.1 | 22.2 | -0.4 | -7.0 | 16.4 |
| | | 2090s | -14.8 | -16.0 | 21.4 | -6.2 | -44.7 | -46.9 | -17.9 |
| | RCP45 | 2050s | 41.3 | 44.4 | 87.9 | 50.4 | 0.2 | 15.5 | 40.0 |
| | | 2090s | 27.1 | 10.5 | 79.9 | 24.1 | -29.1 | -25.0 | 14.6 |
| | RCP85 | 2050s | 31.5 | 21.1 | 65.8 | 60.5 | -16.9 | -14.2 | 24.6 |
| | | 2090s | 44.1 | 24.6 | 103.1 | -12.4 | -42.1 | -47.2 | 11.7 |
| RCM10 | RCP45 | 2050s | -24.3 | -22.2 | -22.0 | -46.8 | -58.2 | -46.0 | -36.6 |
| | | 2090s | 78.7 | 88.7 | 149.9 | 56.2 | -12.9 | -14.9 | 57.6 |
| | RCP85 | 2050s | -0.1 | 24.3 | 26.8 | -15.3 | -39.7 | -34.5 | -6.4 |
| | | 2090s | -31.1 | -69.0 | -78.9 | -85.0 | -85.8 | -83.3 | -72.2 |
| RCM16 | RCP45 | 2050s | 57.0 | 46.3 | 28.8 | -0.4 | -24.2 | -29.0 | 13.1 |
| | | 2090s | 82.1 | 89.1 | 32.1 | 1.0 | -30.9 | -33.8 | 23.3 |
| | RCP85 | 2050s | -19.5 | -44.2 | -66.1 | -41.0 | -19.5 | -34.7 | -37.5 |
| | | 2090s | 155.6 | 129.1 | 11.6 | -49.4 | -69.0 | -69.3 | 18.1 |
| Ensemble | RCP45 | 2050s | 13.4 | 7.6 | 20.6 | 13.3 | -19.7 | -21.7 | 2.2 |
| | | 2090s | 25.6 | 30.3 | 46.2 | 22.6 | -26.7 | -30.0 | 11.3 |
| | RCP85 | 2050s | 1.6 | 27.6 | 47.5 | 12.6 | -33.3 | -32.7 | 3.9 |
| | | 2090s | 16.3 | 76.2 | 52.9 | -43.0 | -63.5 | -65.2 | -4.4 |

| | |
|---|---|
| | -100% |
| | -75 |
| | -50 |
| | -25 |
| | 0 |
| | 25 |
| | 50 |
| | 75 |
| | 100% |

Changes in future climate induce significant variations in monthly runoff especially during pre-monsoon (April-June) and monsoon seasons (July-September). During the spring season, the streamflow is normally generated due to snowmelt with small contributions from the rainfall, whereas during monsoon periods, streamflow is dominated by glacier melt with monsoon precipitation.

The mean monthly changes in streamflow during the melting season between April to September for both future time periods with respect to reference (960 mm) is provided in Table 5. The largest increment in projected streamflow is found during the pre-monsoon season under RCP 4.5 and RCP 8.5 in all selected models and their ensembles. Under RCP 2.6, the streamflow shows the largest increase in projected streamflow during pre-monsoon 25.3 to 33.1 % while a downward trend –7% during the monsoon in near future and a stronger decrease in the far future period up to –46.9 %. For RCP 4.5, streamflow evident multi model ensemble mean increasing rate (13.8 %) during pre-monsoon (April-June) in both future periods and it is more pronounced (34.1 %) by the end of the century. Similarly, under RCP 8.5, projected streamflow also exhibited substantial mean rise in streamflow in both future periods (25.6 % and 48.4 %, respectively). Almost all RCM-simulations and their ensembles show substantial decline of streamflow during monsoon despite significant increases in streamflow being found for the observed period. For RCP 4.5, the multi-model ensemble mean streamflow during the monsoon season is projected to decrease by –9.4 % to –11.4 % during near 2040–2059 and far future 2080–2099 periods respectively, which is even more accentuated for RCP 8.5, with –17.8 % in 2050 s and –57.2 % in 2080–2099. Such decrease in streamflow rate during monsoon is mainly linked to the bilateral relationship between significant increase in temperature and early onset of snow and glacier melt during pre-monsoon (April-June: snow melt followed by extreme events in conjunction with glacier melt). Consequently, one month earlier peak flow pre-monsoon is found under RCP 4.5 in both future periods whereas the peak streamflow shifted to late pre-monsoon (June) compared to the reference (August) under RCP 8.5 by the end of the century.

Several factors may contribute to these substantial shifts in the hydrological regime, including regional hydroclimatic factors and the physical characteristics (presence of snow and glaciers) of the study region. The Naltar catchment is mainly characterized by snow fed-glacierized catchment with major influence of the westerlies. During the pre-monsoon period, there is a significant rise in temperature, and solid precipitation occurs in high altitudes during the reference period; this precipitation could occur in a liquid state during the scenario periods. It may result in the occurrence of earlier peak cryosphere melt with varying magnitude during the pre-monsoon in both future periods under the considered RCPs. Results from our PDSLIM and the conceptual LRM models for intra-seasonal streamflow changes are consistent with projections developed by Lutz et al. (2016) using the Spatial Processes in Hydrology (SPHY) model, Azmat et al. (2020) using multiple models in Hunza and Mishra et al. (2020) in two sub-catchments of HMA (Naltar in Karakoram and Trishuli in Nepal). Due to varying scenarios, climate and hydrological models adopted, it is difficult to make a direct, quantitative comparison. Overall, intra-annual potential change in streamflow shows a substantial and consistent alteration in the hydrological regime of the Naltar catchment attaining decline of peak flows one-two months earlier than the current natural conditions.

### 3.8. Projected change in hydrological components on net streamflow

The impact of climate change on the hydrological components (glacier runoff, surface runoff and sub-surface runoff) on net streamflow during the melting season is of high importance especially in a snow and glacier dominated catchment. Table 6 depicts the relative change in individual hydrological contributions to the net flow for all RCMs and their multi-model ensemble mean during both future periods relative to the observed period. The projected contribution of individual components to total runoff simulated by RCM9 under RCP 2.6 and multi-model ensemble mean under RCP 4.5 and RCP 8.5 for both future periods relative to present are given in Fig.9.

The relative change in each contribution simulated by RCMs is significantly different from each other as shown in Table 6. Overall, the results indicate that the direct surface runoff will contribute to the future

**Table 6**
Hydrological contributions to the Naltar streamflow for individual CORDEX climate models and their ensemble mean considering RCP 2.6, RCP 4.5 and RCP 8.5 climate scenarios using PDSLIM and LRM.

| RCP | | 1991–2010 to 2040–2059 | | | | | | 1991–2010 to 2080–2099 | | | | | |
|---|---|---|---|---|---|---|---|---|---|---|---|---|---|
| | | Glacier Runoff (mm) | | Surface Runoff (mm) | | Sub-surface Runoff (mm) | | Glacier Runoff (mm) | | Surface Runoff (mm) | | Sub-surface Runoff (mm) | |
| | **Reference** | **368** | | **177** | | **416** | | **368** | | **177** | | **416** | |
| | MODEL | Value | Change | Value | Change | Value | Change | Value | Change | Value | Change | Value | Change |
| | | mm | % | mm | % | mm | % | mm | % | mm | % | mm | % |
| **RCP26** | *RCM9* | *259* | *−29.6* | *248* | *40.1* | *563* | *35.3* | *177* | *−51.9* | *169* | *−4.5* | *402* | *−3.4* |
| **RCP45** | RCM1 | 266 | −27.7 | 239 | 35.2 | 507 | 21.8 | 177 | −51.9 | 270 | 52.7 | 555 | 33.3 |
| | RCM2 | 323 | −12.2 | 246 | 38.7 | 500 | 20.2 | 225 | −38.8 | 317 | 78.9 | 600 | 44.2 |
| | RCM3 | 183 | −50.2 | 236 | 33.2 | 457 | 9.8 | 136 | −63.2 | 266 | 50.4 | 502 | 20.7 |
| | RCM4 | 181 | −50.7 | 227 | 28.1 | 454 | 9.0 | 155 | −58.0 | 261 | 47.5 | 543 | 30.6 |
| | RCM5 | 175 | −52.4 | 212 | 19.9 | 445 | 7.0 | 114 | −68.9 | 230 | 29.9 | 476 | 14.3 |
| | RCM6 | 223 | −39.3 | 195 | 10.2 | 403 | −3.2 | 141 | −61.8 | 216 | 22.2 | 468 | 12.6 |
| | RCM7 | 215 | −41.7 | 282 | 59.2 | 611 | 46.9 | 199 | −45.9 | 349 | 97.0 | 710 | 70.7 |
| | RCM8 | 239 | −35.0 | 257 | 44.9 | 553 | 33.0 | 202 | −45.2 | 337 | 90.4 | 640 | 53.8 |
| | RCM9 | *314* | *−14.7* | *333* | *88.0* | *642* | *54.2* | *193* | *−47.6* | *280* | *58.4* | *555* | *33.3* |
| | RCM10 | 243 | −34.0 | 102 | −42.3 | 210 | −49.6 | 217 | −41.0 | 395 | 123.1 | 749 | 80.0 |
| | RCM16 | 229 | −37.7 | 233 | 31.7 | 501 | 20.5 | 160 | −56.4 | 289 | 63.5 | 552 | 32.7 |
| | **Ensemble** | **230** | **−37.6** | **231** | **30.5** | **481** | **15.7** | **168** | **−54.3** | **275** | **55.4** | **550** | **32.2** |
| **RCP85** | RCM1 | 198 | −46.3 | 240 | 35.6 | 487 | 17.1 | 127 | −65.4 | 215 | 21.2 | 409 | −1.7 |
| | RCM2 | 345 | −6.2 | 250 | 41.5 | 509 | 22.3 | 126 | −65.8 | 212 | 19.5 | 417 | 0.2 |
| | RCM3 | 158 | −57.2 | 242 | 36.6 | 493 | 18.5 | 121 | −67.2 | 237 | 33.7 | 455 | 9.3 |
| | RCM4 | 253 | −31.3 | 207 | 17.1 | 472 | 13.5 | 100 | −72.9 | 182 | 2.6 | 396 | −4.9 |
| | RCM5 | 446 | 21.2 | 257 | 45.1 | 547 | 31.4 | 87 | −76.4 | 185 | 4.5 | 378 | −9.2 |
| | RCM6 | 157 | −57.4 | 191 | 7.8 | 353 | −15.3 | 102 | −72.2 | 156 | −12.1 | 254 | −39.0 |
| | RCM7 | 149 | −59.4 | 255 | 44.3 | 535 | 28.7 | 117 | −68.3 | 342 | 93.0 | 664 | 59.6 |
| | RCM8 | 188 | −48.9 | 240 | 35.5 | 421 | 1.1 | 128 | −65.1 | 260 | 46.8 | 471 | 13.1 |
| | RCM9 | *242* | *−34.3* | *313* | *76.7* | *598* | *43.9* | *123* | *−66.5* | *272* | *53.9* | *533* | *28.0* |
| | RCM10 | 221 | −40.0 | 198 | 12.0 | 399 | −4.1 | 125 | −66.0 | 33 | −81.5 | 48 | −88.4 |
| | RCM16 | 59 | −83.9 | 198 | 12.1 | 354 | −14.8 | 109 | −70.3 | 222 | 25.4 | 456 | 9.6 |
| | **Ensemble** | **209** | **−43.3** | **244** | **38.0** | **478** | **15.0** | **114** | **−69.0** | **208** | **17.6** | **410** | **−1.3** |

**Table 7**
Projected water balance components in the melting season simulation for the individual CORDEX climate models and their ensemble mean for the two future periods under RCP 2.6, RCP 4.5 and RCP 8.5. SWE is the snow water equivalent melt during the ablation season.

| RCP | | 2040–2059 | | | | | 2080–2099 | | | | |
|---|---|---|---|---|---|---|---|---|---|---|---|
| | | SWE | Ice melt | Precip. | ET | $Q_{simulated}$ | SWE | Ice melt | Precip. | ET | $Q_{simulated}$ |
| | | mm | mm | mm | mm | mm | Mm | mm | mm | mm | mm |
| | **Reference** | **1294** | **133** | **414** | **664** | **960** | **1294** | **133** | **414** | **664** | **960** |
| | MODEL | | | | | | | | | | |
| **RCP26** | RCM9 | *1671* | *48* | *262* | *720* | *1080* | *1161* | *61* | *227* | *718* | *748* |
| **RCP45** | RCM1 | 1311 | 129 | 363 | 659 | 1012 | 1362 | 72 | 384 | 676 | 1002 |
| | RCM2 | 1330 | 214 | 419 | 683 | 1069 | 1376 | 136 | 434 | 578 | 1142 |
| | RCM3 | 1267 | 42 | 509 | 710 | 876 | 1338 | 38 | 533 | 764 | 904 |
| | RCM4 | 1261 | 48 | 396 | 627 | 862 | 1341 | 53 | 383 | 648 | 959 |
| | RCM5 | 1237 | 39 | 355 | 621 | 833 | 1241 | 17 | 375 | 676 | 820 |
| | RCM6 | 1083 | 125 | 515 | 750 | 821 | 1284 | 54 | 387 | 830 | 825 |
| | RCM7 | 1680 | 38 | 289 | 706 | 1107 | 1761 | 60 | 435 | 762 | 1258 |
| | RCM8 | 1582 | 71 | 269 | 743 | 1049 | 1486 | 91 | 607 | 828 | 1178 |
| | RCM9 | *1532* | *139* | *765* | *801* | *1288* | *1431* | *95* | *431* | *790* | *1028* |
| | RCM10 | 679 | 214 | 503 | 792 | 555 | 1567 | 86 | 772 | 852 | 1360 |
| | RCM16 | 1290 | 89 | 421 | 699 | 964 | 1338 | 54 | 554 | 769 | 1002 |
| | **Ensemble** | **1302** | **91** | **437** | **704** | **942** | **1360** | **64** | **481** | **742** | **993** |
| **RCP85** | RCM1 | 1176 | 105 | 418 | 682 | 925 | 918 | 92 | 415 | 735 | 751 |
| | RCM2 | 1184 | 324 | 451 | 733 | 1104 | 918 | 93 | 384 | 613 | 754 |
| | RCM3 | 1169 | 66 | 563 | 763 | 892 | 918 | 78 | 652 | 771 | 812 |
| | RCM4 | 1184 | 188 | 303 | 778 | 932 | 917 | 62 | 367 | 663 | 677 |
| | RCM5 | 1184 | 429 | 364 | 727 | 1250 | 917 | 44 | 409 | 674 | 649 |
| | RCM6 | 839 | 94 | 513 | 771 | 700 | 696 | 85 | 473 | 1048 | 511 |
| | RCM7 | 1546 | 34 | 272 | 744 | 940 | 1435 | 48 | 545 | 745 | 1122 |
| | RCM8 | 930 | 113 | 773 | 777 | 849 | 1036 | 90 | 677 | 1019 | 859 |
| | RCM9 | *1478* | *133* | *617* | *850* | *1153* | *1154* | *71* | *634* | *833* | *928* |
| | RCM10 | 931 | 167 | 702 | 817 | 818 | 282 | 132 | 622 | 1180 | 206 |
| | RCM16 | 669 | 3 | 644 | 496 | 612 | 917 | 65 | 654 | 883 | 787 |
| | **Ensemble** | **1182** | **126** | **511** | **738** | **931** | **918** | **77** | **536** | **821** | **733** |

more than in the reference period to net streamflow while total streamflow will be substantially influenced also by subsurface runoff, with glacier runoff diminishing as an effect of the glaciers' area shrinkage.

According to RCP 2.6, the results reveal a decline in both surface and glacier runoff in the far future period. In the near future, there is a significant rise in sub-surface runoff, amounting to 35.3 %, which is expected to decrease by 3.4 % in the far future period. Projections for RCP 4.5 indicate that glacier runoff is expected to decrease in all RCMs, with multi-model ensemble mean of –37.6 % and –54.3 % in two future periods. The strongest decrease is found under RCP 8.5 for multi-model ensemble mean up to –43.3% during 2040–2059 and –69 % during 2080–2099. Similarly, projected surface runoff in all considered scenarios is found to be higher than in the reference period except under RCP 2.6 by the end of the century. Under RCP 4.5, the projected surface runoff ensemble contribution to the net streamflow is expected to increase by 55.4 % by the end of the century and by 38 % to 17.6 % under RCP 8.5, still remaining higher than in the reference period. In the Naltar catchment, sub-surface runoff contributes more to the net streamflow through most of the year and this will remain also in the projected future climate. The largest contribution of sub-surface runoff is due to the dominant presence of snowmelt in groundwater storage which returns to streamflow flow through baseflow. The contribution of sub-surface runoff in net streamflow pattern is continued in the future and the maximum contribution (32.2 %) is reached during the far-future period (2080–2099) under RCP 4.5 subsequently steadily declining (–1.3 %) until 2099 with RCP 8.5.

Another reason for the higher contribution of sub-surface runoff in the Naltar catchment, is the gradual reduction of glacier's area in both future periods under three considered RCPs resulting in a substantial contribution of snowmelt to subsurface flow instead of net surface runoff. Hence, seasonal snow provides a considerable amount of melted water. It is also observed that glaciers will still contribute a significant amount to net streamflow in the near future and RCP8.5 until glacier mass depletion reaches a tipping point in the far future period under RCP8.5 with the consequence of a sharp decline in streamflow to just 733 mm compared to the actual 960 mm.

The findings from our hydro-glaciological modeling, indicate an increase in river runoff in the far future with the RCP45 scenario and a decline under the RCP85 scenario. Although dynamics of our results are in agreement with previous studies with earlier shift in snow melt followed by significant increasing trend in glacier shrinkage and anticipation of streamflow peak at large scale (Kraaijenbrink et al. 2017; Rounce et al. 2020) and regional/catchment level (Ali et al., 2018; Azmat et al., 2020; Mishra et al., 2020; Soncini et al., 2015), the variability in hydrological responses appears to be more varied than is normally expected in smaller catchments. There are several factors such as topography, soil characteristics, localized climatic conditions like precipitation intensity and distribution, vegetation cover, scale effects and anthropogenic factors that can be associated with possible differences in the hydrological response in the Naltar catchment. In future research, it would be beneficial to investigate the impact of these factors on the hydrological response of smaller catchments in the HMA region.

### 3.9. Projected change in water balance

The projected water balance was estimated for all individual RCMs and plotted based on a the Truc-Budyko plot (Fig.10), which shows the relationship between the runoff coefficient (Q/P) and the aridity index (P/ETp). Further, projected values of the individual components of the water balance in the melting season, were computed and displayed in Table 6. Under all RCPs, most RCMs and their ensemble mean are projected to break the water limit (Q > P) and are located within the "gaining" domain as shown in Fig.10 (a-f) in both future scenarios. In gaining catchment, where precipitation is not sufficient to close the water balance cycle, additional water is required to close the water balance in the melt season. This additional water can be fed by snow and glacier melting in glacierized catchments or can be supplied by subsurface water stored prior to the melt season. However, because measured streamflow at the beginning of the melt season is very low (indicating a limited subsurface water storage) it is reasonable to conjecture that most of the missing water comes from snow and ice melt

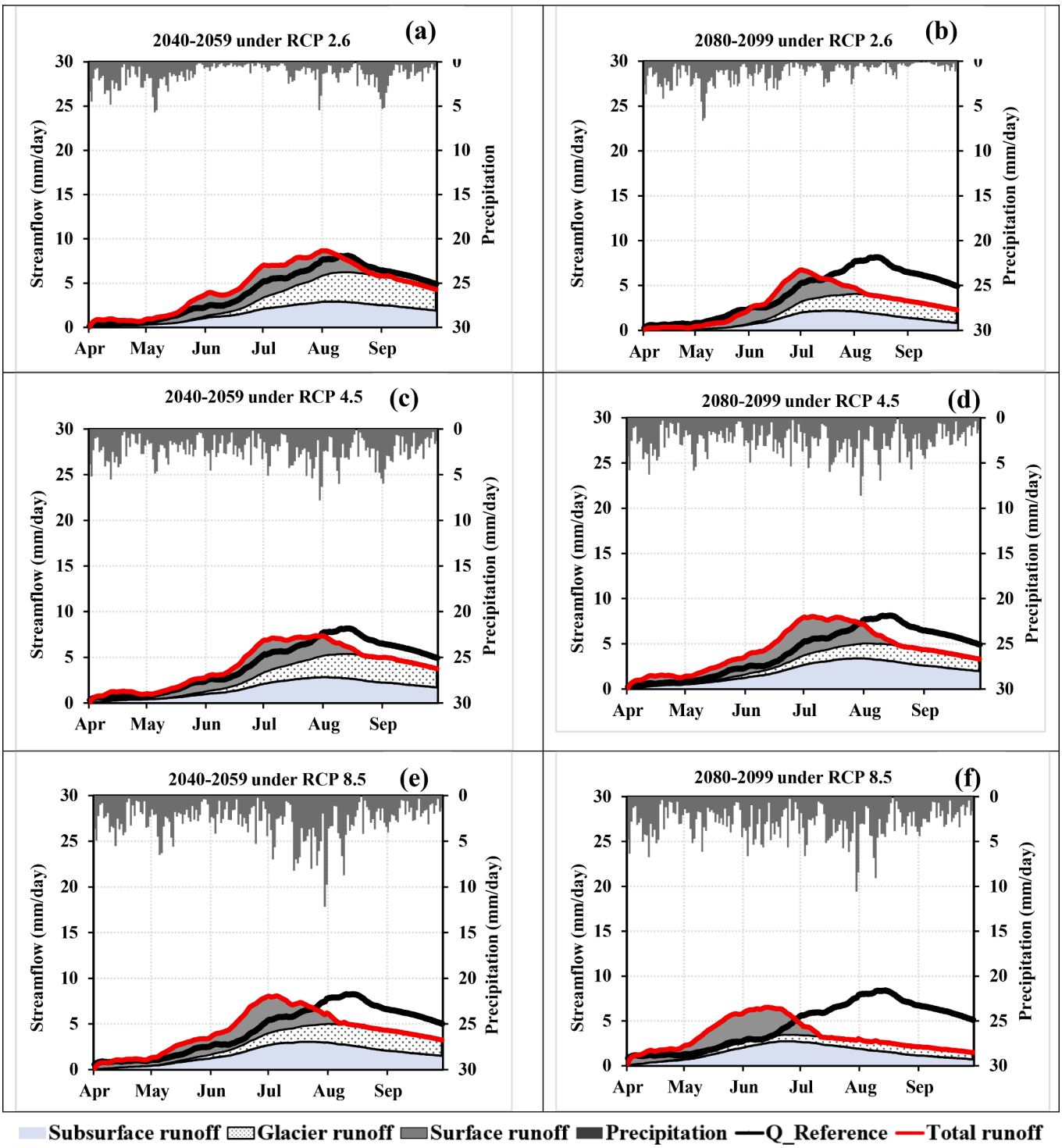


**Fig. 9.** Projected contribution of individual components (subsurface runoff, glacier runoff and surface runoff) to total runoff simulated by for RCM9 under RCP 2.6 and multi-model ensemble mean under RCP 4.5 and RCP 8.5 for 2040–2059 and 2080–2099 relative to reference 2006–2016. Here Q_Reference and exhibits mean observed simulated streamflow during 2006–2016.

and is exacerbated by negative glacier mass balance, as shown in Fig.6 and Fig.7. It is also noticed that RCM10 under RCP 8.5 in the far future period lies below the water limit and the simulated streamflow is likely highly underestimated. Such underestimation is possibly due to the lower projected values of snow depth ratio, being just 0.64 and 0.20, as shown in Table S6 which ultimately impact all glaciological and hydrological simulations, as shown in Fig.5 and Fig.8.

The projections of seasonal mass balance loss also exhibit a significant rise in temperature in both future periods. This increase is expected to be evident across all RCPs. Consequently, less snow melt is available in the future. Additionally, RCMs also projected an increase in precipitation in both future periods (+5.4 % to +29.5 %). Based on such arguments, future climate projections are moving towards the water limit line in both future periods especially under RCP 8.5 (Fig. 8) and there is the possibility that the hydrological regime of Naltar, in the long term, will gradually convert from snow and glacier melt dominance to

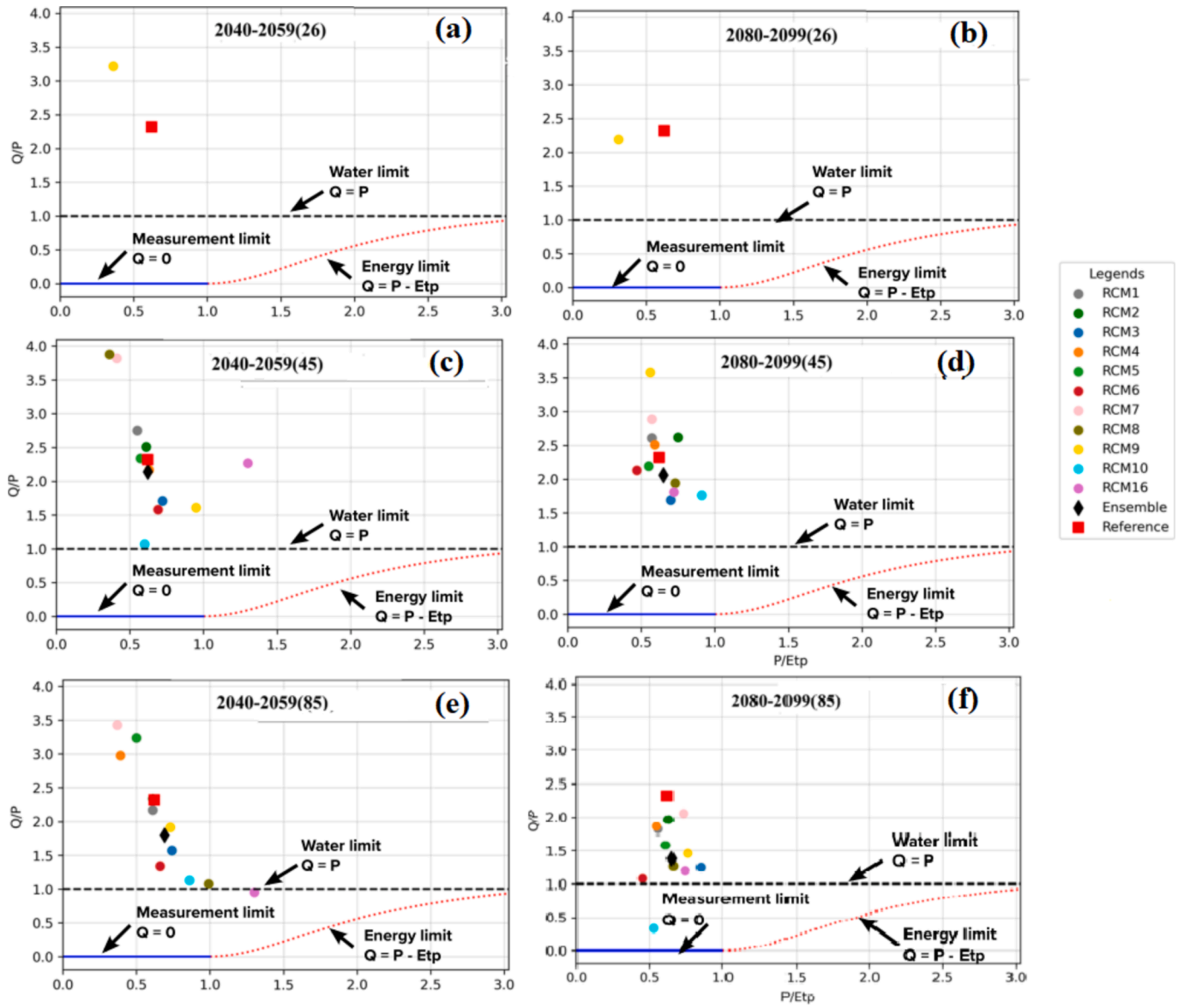


**Fig. 10.** The Turc-Budyko plot for eleven RCMs and their multi-model ensemble mean in two future periods (2040–2059 and 2080–2099). Reference point marked relationship during present condition (2006–2016).

rainfall dominance.

## 4. Summary and conclusions

In the High Mountain Asia (HMA), assessing future hydro-glaciological changes is more complex due to uncertainties associated with the historical and projected climate data, glacier extent, glacier mass balance, and model processes and parameters. In this study, the energy and mass balance model PDSLIM coupled with the conceptual lumped hydrological model LRM, observed hourly meteorological and daily hydrometric data and 37 simulations of RCMs from the CORDEX-WAS44 ensemble were used to estimate the future evolution of glacio-hydrological conditions in the Naltar catchment, located in Hunza, one of largest glacierized region in HMA. By considering a comprehensive spectrum of climatic conditions (the largest available ensemble of models and scenarios) we assessed the range of uncertainties and their relative impact on projected glaciological and hydrological regimes.

The following conclusions can be drawn from the present study. Climate projections exhibit a significant increase in temperature between +0.9 to +6.0 °C and precipitation +5.4 % to +29.5 % from April-September by the end of this century for RCP 2.6, 4.5 and 8.5. A maximum increase in precipitation and temperature is found for 2080–2099 under RCP8.5, with significant changes during pre-monsoon for temperature and early monsoon for precipitation. Snowpack at the end of the winter season is projected to decrease from −6% (RCP 4.5 in the far future) to –37 % (RCP 8.5 in the far future). Solar radiation is also projected to increase in both future periods under RCP 4.5 and 8.5. Although relative humidity, wind speed, and pressure show increasing trends both in the near term and in the long term, the changes of these variables is not as high as that of temperature and precipitation.

Future projections for energy and mass balance indicate that snow and ice melt will consistently increase in both future periods with an early shift in the timing of the maximum snowmelt, as it appears in June during near future (2040–2059) and in May for far future (2080–2099) under the highest emission scenario. Further, projections of glacier mass balance show that the glaciers's extent in the Naltar catchment are expected to shrink from –27 % to –43 % for RCP 2.6, from –41 % to –60 % for RCP 4.5 and from –58 % to –80 % for RCP 8.5 by the near and far future, respectively. Annual mass balance for the investigated glacierized area is assessed to be already negative in the current climate

(–737 mm w.e.) and will worsen in the near future (–887 to –2018 mm w.e. under RCP 4.5 and 8.5, respectively) and far future (–1154 to –2597 mm w.e. for the two RCPs).The glacier extent is expected to change sharply after the 2050s for most glaciers, indicating that glaciers are retreating more rapidly and that some glaciers may disappear by the end of the century thus indicating that the 'Karakoram anomaly' will not save the Naltar's glaciers. Such earlier snowmelt followed by glacier retreat is likely to be a result of the warming over elevated regions, which drives not only to an earlier melting season but also may lead to extreme events, glacier outburst and landslide events in future.

Streamflow availability is projected to change for RCP 4.5 (–2.7 % to + 3.4 %) and decrease (–4% to –23.7 %) for RCP 8.5 with respect to the present climate. Flow composition analysis depicts a decreasing contribution of glacier runoff up to −69 % into net streamflow by the end of the century under RCP 8.5 as an effect of glaciers' area shrinkage (Table 6). Because of the anticipation of the melt season from one to two months earlier by the end of the century the streamflow in the Naltar could be largely increased in the pre-monsoon season and then decrease in the monsoon season in both future periods, and the total summer runoff will not change significantly according to scenario RCP 4.5 while is expected to decrease by –3% and –24 % in the near and far future under RCP 8.5. Using the Turc-Budyko approach, the water energy and mass balance indicates that Naltar's hydrological regime can shift gradually from snow and glacier melt dominance to rainfall dominance.

In light of the above results and discussion, water availability in the Naltar catchment will be highly uncertain by the end of the century in comparison with the current situation. Pakistan is investing in hydropower development in Northern areas to meet energy demand. The results of this study will help the Government and other stakeholders to take informed decisions and assess financial risks for further development of reservoir operations and agriculture on farm water management in downstream areas by considering projected changes both in timing, total streamflow volumes and hydrological regimes driven by climate projections.

## CRediT authorship contribution statement

**Muhammad Usman Liaqat:** Writing – original draft, Validation, Conceptualization. **Ana Casanueva:** Formal analysis, Methodology, Investigation, Validation, Data curation, Software, Visualization, Writing – review & editing. **Rubina Ansari:** Supervision, Visualization, Writing – review & editing. **Giovanna Grossi:** Supervision, Visualization, Writing – review & editing. **Roberto Ranzi:** Formal analysis, Methodology, Investigation, Validation, Visualization, Writing – review & editing.

## Declaration of competing interest

The authors declare that they have no known competing financial interests or personal relationships that could have appeared to influence the work reported in this paper.

## Acknowledgements

The study covers one part of the PhD research work of the first author funded by the University of Brescia, Italy, and the Erasmus (Italy) Traineeship Program. The research was partially funded by the Regione Lombardia and CNR-IRPI grant on debris flow modeling in mountain areas. C.A. acknowledges support from Project COMPOUND (TED2021-131334A-I00) funded by MCIU/AEI/10.13039/501100011033 and by the European Union Next Generation EU/PRTR. The authors highly acknowledged the Water and Power Development Authority (WAPDA) for providing reliable data for our study and helping to publish valuable information. Ned Bair from UC Santa Barbara is thanked for having provided the SWE data for the model's initialisation. The authors are also grateful to the reviewers who helped to improve the original version of the manuscript.

## Appendix A. Supplementary data

Supplementary data to this article can be found online at https://doi.org/10.1016/j.jhydrol.2024.132411.

## Data availability

Data will be made available on request.

## References

Ahmad, B., Rasul, G., 2018. Statistically downscaled projections of CORDEX South Asia using quantile mapping approach over Pakistan region. International Journal of Global Warming 16, 435–460.

Ali, S., Li, D., Congbin, F., Khan, F., 2015. Twenty first century climatic and hydrological changes over Upper Indus Basin of Himalayan region of Pakistan. Environmental Research Letters 10, 014007.

Ali, A.F., Xiao, C.-d., Zhang, X.-p., Adnan, M., Iqbal, M., Khan, G., 2018. Projection of future streamflow of the Hunza River Basin, Karakoram Range (Pakistan) using HBV hydrological model. Journal of Mountain Science 15, 2218–2235.

Ansari, R., Liaqat, M.U., Grossi, G., 2022. Evaluation of gridded datasets for terrestrial water budget assessment in the Upper Jhelum River Basin-South Asia. Journal of Hydrology 613, 128294.

Ansari, R., Liaqat, M.U., Grossi, G., 2024. Improving flood and drought management in transboundary Upper Jhelum Basin-South Asia. Science of the Total Environment 945, 174044.

Atif I, Iqbal J, Su L-j (2019) Modeling hydrological response to climate change in a data-scarce glacierized high mountain Astore Basin using a fully distributed TOPKAPI model Climate 7:127.

Azmat M, Wahab A, Huggel C, Qamar MU, Hussain E, Ahmad S, Waheed A (2020) Climatic and hydrological projections to changing climate under CORDEX-South Asia experiments over the Karakoram-Hindukush-Himalayan water towers Science of the Total Environment 703:135010.

Berthier, É., Brun, F., 2019. Karakoram geodetic glacier mass balances between 2008 and 2016: persistence of the anomaly and influence of a large rock avalanche on Siachen Glacier. Journal of Glaciology 65, 494–507.

Bishop, M.P., Shroder, J.F., Ali, G., Bush, A.B., Haritashya, U.K., Roohi, R., Sarikaya, M. A., Weihs, B.J., 2014. Remote sensing of glaciers in Afghanistan and Pakistan. In: Kargel, J.S., Leonard, G.J., Bishop, M.P., Kääb, A., Raup, B.H. (Eds.), Global Land Ice Measurements from Space. Springer, Berlin Heidelberg, Berlin, Heidelberg, pp. 509–548.

Bocchiola D, Diolaiuti G, Soncini A, Mihalcea C, D'agata C, Mayer C, Lambrecht A, Rosso R, Smiraglia C (2011) Prediction of future hydrological regimes in poorly gauged high altitude basins: the case study of the upper Indus, Pakistan.

Bokhari, S.A.A., Ahmad, B., Ali, J., Ahmad, S., Mushtaq, H., Rasul, G., 2018. Future climate change projections of the Kabul River Basin using a multi-model ensemble of high-resolution statistically downscaled data Earth Systems. Environment 2, 477–497.

Bosshard, T., Kotlarski, S., Ewen, T., Schär, C., 2011. Spectral Representation of the Annual Cycle in the Climate Change Signal Hydrology Earth System Sciences 15, 2777–2788.

Budyko, M.I., Miller, D.H., Miller, D.H., 1974. Climate and Life, vol 508. Academic press New York.

Carturan, L., Baroni, C., Brunetti, M., Carton, A., Dalla Fontana, G., Salvatore, M.C., Zanoner, T., Zuecco, G., 2016. Analysis of the Mass Balance Time Series of Glaciers in the Italian Alps the Cryosphere 10, 695–712.

Chen, H., Xiong, J., Cui, P., Chen, X., Ge, Y., Fang, C., Zhang, B., Yang, T., Khan, I., 2024. Causes and dynamic change characteristics of the 2022 devastating floods in Pakistan. Natural Hazards 1–21.

Choudhary, A., Dimri, A., 2018. Assessment of CORDEX-South Asia Experiments for Monsoonal Precipitation over Himalayan Region for Future Climate Climate Dynamics 50, 3009–3030.

Christensen JH, Boberg F, Christensen OB, Lucas-Picher P (2008) On the need for bias correction of regional climate change projections of temperature and precipitation Geophysical research letters 35.

Coron, L., Andréassian, V., Perrin, C., Le Moine, N., 2015. Graphical tools based on Turc-Budyko plots to detect changes in catchment behaviour. Hydrological Sciences Journal 60, 1394–1407.

DAWN (2021) 4 people missing as glacial surge blocks nullah in Naltar DAWN News Paper doi:https://www.dawn.com/news/1633418.

Fang, X., Pomeroy, J.W., 2023. Simulation of the impact of future changes in climate on the hydrology of Bow River headwater basins in the Canadian Rockies. Journal of Hydrology 620, 129566.

Farinotti, D., Immerzeel, W.W., de Kok, R.J., Quincey, D.J., Dehecq, A., 2020. Manifestations and mechanisms of the Karakoram glacier Anomaly. Nature Geoscience 13, 8–16.

Fatima, E., Hassan, M., 2020. Hasson Su, Ahmad B, Ali SSF. Future Water Availability from the Western Karakoram under Representative Concentration Pathways as Simulated by CORDEX South Asia Theoretical and Applied Climatology 141, 1093–1108.

Fowler H, Kilsby C, O'Connell P (2003) Modeling the impacts of climatic change and variability on the reliability, resilience, and vulnerability of a water resource system Water Resources Research 39:8, 1222.
Gardezi, H., Xing, A., Bilal, M., Zhuang, Y., Muhammad, S., Janjua, S., 2022. Preliminary investigation and dynamic analysis of a multiphase ice-rock avalanche on July 5, 2021, in the upper Naltar valley. Gilgit, Pakistan Landslides 19, 451–463.
Giorgi, F., Jones, C., Asrar, G.R., 2009. Addressing climate information needs at the regional level: the CORDEX framework World Meteorological Organization. Bulletin 58, 175.
Giorgi, F., Coppola, E., Solmon, F., Mariotti, L., Sylla, M., Bi, X., Elguindi, N., Diro, G., Nair, V., Giuliani, G., 2012. RegCM4: model description and preliminary tests over multiple CORDEX domains. Climate Research 52, 7–29.
Godwin-Austen, H.H., 1864. On the glaciers of the Mustakh Range The. Journal of the Royal Geographical Society of London 34, 19–56.
Grossi G, Caronna P, Ranzi R (2013) Hydrologic vulnerability to climate change of the Mandrone glacier (Adamello-Presanella group, Italian Alps) Advances in water resources 55:190-203. https://doi.org/10.1016/j.advwatres.2012.11.014.
Grossi, G., Falappi, L., 2003. Comparison of energy fluxes at the land surface-atmosphere interface in an Alpine valley as simulated with different models. Hydrol. Earth Syst. Sci. 7 (6), 920–936. https://doi.org/10.5194/hess-7-920-2003.
Hasson Su, Böhner J (2019) Hydrological Cycle Over the Indus Basin at Monsoon Margins: Present and Future. In: Indus River Basin. Elsevier, pp 245-264.
Hasson, S., Saeed, F., Böhner, J., Schleussner, C.-F., 2019. Water availability in Pakistan from Hindukush–Karakoram–Himalayan watersheds at 1.5 C and 2 C Paris Agreement targets. J Advances in Water Resources 131, 103365.
Hayden, H., 1907. Notes on certain glaciers in Northwest Kashmir Rec. Geol. Surv. India 35, 127–137.
Hewitt, K., 2005. The Karakoram anomaly? Glacier expansion and the 'elevation effect,. Karakoram Himalaya Mountain Research Development 25, 332–340.
Huss, M., Hock, R., 2015. A new model for global glacier change and sea-level rise. *Frontiers in Earth Science* 3, 54.
Hussain, M., Mumtaz, S., 2014. Climate change and managing water crisis: Pakistan's perspective J. Reviews on Environmental Health 29, 71–77.
Ismail, M.F., Naz, B.S., Wortmann, M., Disse, M., Bowling, L.C., Bogacki, W., 2020. Comparison of two model calibration approaches and their influence on future projections under climate change in the Upper Indus Basin. Climatic Change 163, 1227–1246.
Iturbide, M., Fernández, J., Gutiérrez, J.M., et al., 2022. Implementation of FAIR principles in the IPCC: the WGI AR6 Atlas repository. Sci Data 9, 629. https://doi.org/10.1038/s41597-022-01739-y.
Jury, M.W., Mendlik, T., Tani, S., Truhetz, H., Maraun, D., Immerzeel, W.W., Lutz, A.F., 2020. Climate projections for glacier change modelling over the Himalayas. International Journal of Climatology 40, 1738–1754.
Katragkou, E., Sobolowski, S.P., Teichmann, C., Solmon, F., Pavlidis, V., Rechid, D., Hoffmann, P., Fernandez, J., Nikulin, G., Jacob, D., 2024. Delivering an improved framework for the new generation of CMIP6-driven EURO-CORDEX regional climate simulations. Bulletin of the American Meteorological Society 105 (6), E962–E974.
Khan, A.J., Koch, M., Tahir, A.A.J.S., 2020. Impacts of Climate Change on the Water Availability, Seasonality and Extremes in the Upper Indus Basin (UIB) 12, 1283.
Kiani, R.S., Ali, S., Ashfaq, M., Khan, F., Muhammad, S., Reboita, M.S., Farooqi, A., 2021. Hydrological projections over the Upper Indus Basin at 1.5° C and 2.0° C temperature increase. Science of the Total Environment 788, 147759.
Knutti, R., Furrer, R., Tebaldi, C., Cermak, J., Meehl, G.A., 2010. Challenges in combining projections from multiple climate models. Journal of Climate 23 (10), 2739–2758.
Kraaijenbrink, P.D., Bierkens, M., Lutz, A., Immerzeel, W., 2017. Impact of a global temperature rise of 1.5 degrees Celsius on Asia's glaciers. Nature 549, 257–260.
Kraaijenbrink, P.D., Stigter, E.E., Yao, T., Immerzeel, W.W., 2021. Climate change decisive for Asia's snow meltwater supply. Nature Climate Change 11, 591–597.
Laghari, A.N., Vanham, D., Rauch, W., 2012. The Indus basin in the framework of current and future water resources management Hydrology Earth System. Sciences 16, 1063–1083.
Liaqat, M.U., Grossi, G., Hasson, S., Ranzi, R., 2022. Characterization of Interannual and Seasonal Variability of Hydro-Climatic Trends in the Upper Indus Basin Theoretical Applied Climatology 147, 1163–1184. https://doi.org/10.1007/s00704-021-03850-3.
Liaqat, U., Ranzi, R., 2024. Distributed modelling of snow and ice melt in the Naltar Catchment, Upper Indus basin. Journal of Hydrology 643, 131935. https://doi.org/10.1016/j.jhydrol.2024.131935.
Lutz AF, Immerzeel W, Kraaijenbrink P, Shrestha AB, Bierkens MF (2016) Climate change impacts on the upper Indus hydrology: Sources, shifts and extremes PloS one 11:e0165630.
Lutz, A., Immerzeel, W., Shrestha, A., Bierkens, M., 2014. Consistent increase in High Asia's runoff due to increasing glacier melt and precipitation. Nature Climate Change 4, 587–592.
Minora, U., Bocchiola, D., D'Agata, C., Maragno, D., Mayer, C., Lambrecht, A., Mosconi, B., Vuillermoz, E., Senese, A., Compostella, C., 2013. 2001–2010 glacier changes in the Central Karakoram National Park: a contribution to evaluate the magnitude and rate of the" Karakoram anomaly". The Cryosphere Discussions 7, 2891–2941.
Minora U, Bocchiola D, D'Agata C, Maragno D, Mayer C, Lambrecht A, Vuillermoz E, Senese A, Compostella C, Smiraglia C (2016) Glacier area stability in the Central Karakoram National Park (Pakistan) in 2001–2010: the "Karakoram Anomaly" in the spotlight Progress in Physical Geography 40:629-660.
Mishra, S.K., Veselka, T.D., Prusevich, A.A., Grogan, D.S., Lammers, R.B., Rounce, D.R., Ali, S.H., Christian, M.H., 2020. Differential impact of climate change on the hydropower economics of two river basins in high mountain Asia. Frontiers in Environmental Science 8, 26.
Muhammad S, Thapa A (2021) Daily Terra–Aqua MODIS cloud-free snow and Randolph Glacier Inventory 6.0 combined product (M* D10A1GL06) for high-mountain Asia between 2002 and 2019 Earth System Science Data 13:767-776.
Nanditha, J.S., Kushwaha, A.P., Singh, R., Malik, I., Solanki, H., Chuphal, D.S., Dangar, S., Mahto, S.S., Vegad, U. and Mishra, V., 2023. The Pakistan flood of August 2022: causes and implications. Earth's Future, 11(3), p.e2022EF003230.
Oreskes, N., Shrader-Frechette, K., Belitz, K., 1994. Verification, validation, and confirmation of numerical models in the earth sciences. Science 263 (5147), 641–646.
Paul, F., Arnaud, Y., Ranzi, R., Rott, H., 2014. European Alps. In: Kargel, J.S., Leonard, G. J., Bishop, M.P., Kääb, A., Raup, B.H. (Eds.), Global Land Ice Measurements from Space. Springer, Berlin Heidelberg, Berlin, Heidelberg, pp. 439–463. https://doi.org/10.1007/978-3-540-79818-7_20.
Prabnakorn, S., Suryadi, F., Chongwilaikasem, J., De Fraiture, C., 2019. Development of an integrated flood hazard assessment model for a complex river system: a case study of the Mun River Basin. Thailand Modeling Earth Systems Environment 5, 1265–1281.
Räisänen, J., Räty, O., 2013. Projections of Daily Mean Temperature Variability in the Future: Cross-Validation Tests with ENSEMBLES Regional Climate Simulations Climate Dynamics 41, 1553–1568.
Ranzi R, Rosso R (1991) Physically based approach to modelling distributed snowmelt in a small alpine catchment IAHS PUBL, IAHS, WALLINGFORD:141-150 https://iahs.info/uploads/dms/8846.141-150-205-Ranzi.pdf.
Ranzi, R., Grossi, G., Iacovelli, L., & Taschner, S. (2004). Use of multispectral ASTER images for mapping debris-covered glaciers within the GLIMS project. In IGARSS 2004. 2004 IEEE International Geoscience and Remote Sensing Symposium (Vol. 2, pp. 1144-1147). IEEE. doi: 10.1109/IGARSS.2004.1368616.
Ranzi, R., Grossi, G., Gitti, A., Taschner, S., 2010. Energy and mass balance of the mandrone glacier (Adamello, Central Alps). Geogr. Fis. Din. Quat. 33, 45–60. https://www.gfdq.glaciologia.it/index.php/GFDQ/article/view/259.
Räty, O., Räisänen, J., Ylhäisi, J.S., 2014. Evaluation of Delta Change and Bias Correction Methods for Future Daily Precipitation: Intermodel Cross-Validation Using ENSEMBLES Simulations Climate Dynamics 42, 2287–2303.
Romshoo, S.A., Marazi, A., 2022. Impact of climate change on snow precipitation and streamflow in the Upper Indus Basin ending twenty-first century. Climatic Change 170, 1–20.
Rounce, D.R., Hock, R., Shean, D.E., 2020. Glacier mass change in High Mountain Asia through 2100 using the open-source python glacier evolution model (PyGEM). Frontiers in Earth Science 7, 331.
Samuelsson P, Jones CG, Willén U, Ullerstig A, Gollvik S, Hansson U, Jansson E, Kjellström M C, Nikulin G, Wyser K (2011) The Rossby Centre Regional Climate model RCA3: model description and performance Tellus A: Dynamic Meteorology Oceanography 63:4-23.
Sebok E, Henriksen HJ, Pastén-Zapata E, Berg P, Thirel G, Lemoine ., Lira-Loarca A, Photiadou C, Pimentel R, Royer-Gaspard ., Kjellström E. Christensen JH Vidal JP, Lucas-Picher P, Donat MG, Besio G, Polo MJ, Stisen S, Caballero Y, Pechlivanidis IG, Troldborg L, Refsgard JC (2022) Use of expert elicitation to assign weights to climate and hydrological models in climate impact studies. Hydrology and Earth System Sciences, 26(21), pp.5605-5625.
Shah, M.I., Khan, A., Akbar, T.A., Hassan, Q.K., Khan, A.J., Dewan, A., 2020. Predicting Hydrologic Responses to Climate Changes in Highly Glacierized and Mountainous Region Upper Indus Basin Royal Society Open Science 7, 191957.
Shakoor, A., Ejaz, N., 2019. Flow Analysis at the Snow Covered High Altitude Catchment via Distributed Energy Balance Modeling Scientific Reports 9, 1–14.
Sobolowski, S., Somot, S., Fernandez, J., Evin, G., Maraun, D., Kotlarski, S., Jury, M., Benestad, R.E., Teichmann, C., Christensen, O.B. and Bülow, K., 2023. EURO-CORDEX CMIP6 GCM selection & ensemble design: Best practices and recommendations.
Soncini, A., Bocchiola, D., Confortola, G., Bianchi, A., Rosso, R., Mayer, C., Lambrecht, A., Palazzi, E., Smiraglia, C., Diolaiuti, G., 2015. Future hydrological regimes in the upper indus basin: A case study from a high-altitude glacierized catchment. Journal of Hydrometeorology 16, 306–326.
Soncini, A., Bocchiola, D., Confortola, G., Minora, U., Vuillermoz, E., Salerno, F., Viviano, G., Shrestha, D., Senese, A., Smiraglia, C., 2016. Future hydrological regimes and glacier cover in the Everest region: The case study of the upper Dudh Koshi basin. Science of the Total Environment 565, 1084–1101.
Stevens, B., Bony, S., 2013. What are climate models missing? Science 340, 1053–1054.
Tahir, A.A., Chevallier, P., Arnaud, Y., Neppel, L., Ahmad, B., 2011. Modeling snowmelt-runoff under climate scenarios in the Hunza River basin. Karakoram Range, Northern Pakistan Journal of Hydrology 409, 104–117.
Tebaldi, C., Knutti, R., 2007. The use of the multi-model ensemble in probabilistic climate projections. Philosophical Transactions of the Royal Society a: Mathematical, Physical and Engineering Sciences 365 (1857), 2053–2075.
Teichmann, C., Eggert, B., Elizalde, A., Haensler, A., Jacob, D., Kumar, P., Moseley, C., Pfeifer, S., Rechid, D., Remedio, A.R., 2013. How does a regional climate model modify the projected climate change signal of the driving GCM: a study over different CORDEX regions using REMO. Atmosphere 4, 214–236.
Teutschbein, C., Seibert, J., 2012. Bias Correction of Regional Climate Model Simulations for Hydrological Climate-Change Impact Studies: Review and Evaluation of Different Methods Journal of Hydrology 456, 12–29.
Turc, L., 1955. Le Bilan D'eau Des Sols: Relations Entre Les Précipitations, L'évaporation et L'écoulement Journées De L'hydraulique 3, 36–44.

Xiang, Y., Zeng, C., Zhang, F., Wang, L., 2024. Effects of climate change on runoff in a representative Himalayan basin assessed through optimal integration of multi-source precipitation data. Journal of Hydrology: Regional Studies 53, 101828.
Zekollari, H., Huss, M., Farinotti, D., 2019. Modelling the future evolution of glaciers in the European Alps under the EURO-CORDEX RCM ensemble. *The Cryosphere* 13 (4), 1125–2114.
Zheng, H., Chiew, F.H., Charles, S., Podger, G., 2018. Future climate and runoff projections across South Asia from CMIP5 global climate models and hydrological modelling. Journal of Hydrology: Regional Studies 18, 92–109.